ETH
Eidgenössische Technische Hochschule Zürich
Swiss Federal Institute of Technology Zurich

DERDW
Department of Earth Sciences

3D geometry and deformation of the Maggia Nappe and the transition to the Southern Steep Belt

Master Thesis

Sascha Winterberg

Supervisors:

Prof. Dr. Neil Mancktelow
Institute of Geology, ETH Zürich

Dr. Eric Reusser
Institute of Geochemistry and Petrology, ETH Zürich

2014

Table of contents

Table of figures

Abstract

Contradictory models of the tectonic nappe succession in the Lepontine dome are published. The area of the Southern Steep Belt where the Maggia Cross Fold bends into the Insubric Fault is only sparsely studied. This thesis uses new acquired field observation and a 3D model to analyze the region between Valle Verzasca, Piano di Magadino and Bellinzona. Foliation observations show the bending of the Southern Steep Belt from almost flat in the north to steep or overturned in the south. The Maggia Cross Fold is influencing the Steep Belt by bending it around a vertical axis. Measurements of intersection and mineral lineations show sub-horizontal east-west orientations that split up in the eastern parts into an additional steeper lineation. The majority of vergences of parasitic folds indicate an antiform in the south. Fold style and relationships require at least three deformation phases that most likely overlapped in time. GeoModeller was used to model two different nappe correlations. Foliation data was assumed to follow nappe boundaries. But modelling in such a manner cannot represent all observed structures. Structures visible only outlined by petrological mapping but not in the foliation orientation could not be modelled. Profiles drawn by hand show the interpretation of this structure. A new Alpine tectonic concept explaining cross folds and the almost simultaneous deformation ages caused by plate relaxation is proposed.

Zusammenfassung

Es wurden wiedersprüchliche Modelle über die tektonische Abfolge der Decken im Lepontinischen Dom publiziert. Das Gebiet der südliche Steilzone wo die Maggia Querfaltung in die Insubrische Linie einbiegt, ist kaum untersucht. Diese Arbeit verwendet neue Feldbeobachtungen und ein 3D Modell um die Region zwischen Verzascatal, Magadinoebene und Bellenz zu analisieren. Schieferungsmessungen zeigen die Umbiegung zur Steilzone von flach im Norden zu steil oder überkippt im Süden. Die Maggia Querfaltung beeinflusst die Steilzone indem sie sie um eine vertikale Achse umfaltet. Intersektionslineare und Minerallineare haben subhorizontale Ost West Ausrichtung die im östlichen Teil durch ein weiteres steiles Linear ergänzt wird. Die meisten Vergenzen der Parasitärfalten zeigen, dass die Antiformen im Süden sind. Der Stil der Falten und deren Beziehungen setzen mindestens drei Deformationsphasen voraus, die sich ziemlich sicher zeitlich überlappten. Mit GeoModeller wurden zwei verschiedene Deckenkorelationen modelliert. Es wurde angenommen, dass die Deckengrenzen der Schieferung folgen. Aber diese Modellierungsannahme kann nicht alle Strukturen darstellen. Strukturen, die nur in petrologische Aufnahmen sichtbar sind aber keine Schieferung haben, können nicht modelliert werden. Manuell erstellte Profile zeigen die Interpretation dieser Strukturen. Ein alpines tektonisches Konzept wird vorgestellt, dass die Querfalten und die beinahe Gleichzeitigkeit der Verfaltungen erklärt.

Introduction

Alpine overview

The Alps are a mountain range extending east-west from Vienna to Nice and Corsica. The Tethys Ocean started closing 65 Ma ago with a SE dipping subduction system. Until 35 Ma the south dipping subduction closed the ocean and the Alps then started forming. The orogen is divided into four main domains. There are the overlying Austroalpine and the non-metamorphic Southern Alps. The Helvetic domain belongs to the northern continental margin that is represented by carbonatic sediments and marls. The Helvetic Nappes were overthrusted by the Penninic domain which contains all sediments from the Tethys Ocean. Internally this domain is heterogeneous: The north Penninic domain originated in a deep marine trough called the Valais trough separated from the main oceanic deep by the Briançonnais which is also named the middle Penninic domain. The main spreading ridge of the plate boundary was in the Piemont-Ligurian Ocean also named south Penninic. It is under discussion how much spreading happened in the Valais trough and whether ophiolites were present (e.g. PFIFFNER 2009; SCHMID et al. 2004). The spreading situation can be compared with the ridges of Baja California (STOCK and HODGES 1989). The Sub Penninic refers to the formerly called *Wurzelzone* (e.g. WENK 1955) or root zone of the nappes and is basically the crystalline basement of the aforesaid Penninic Nappes (MILNES 1974; SCHMID et al. 2004). They contain a longer deformation history than the sediments covering them because they were involved in pre-Alpine orogenies. Thrusting and shearing reduced the thickness of south penninic nappe separators – some are even absent. The absence of this primary evidence for nappe separation makes it very complicated to separate different nappes in the Sub Penninic. Authors like WENK (1953) therefore proposed to expand separation criterions to petrology by defining a core (*Kern*) of gneiss and an envelope (*Hülle*) of schist. The latest attempts to define and correlate nappes by MAXELON and MANCKTELOW (2005) and STECK et al. (2013) led to nappe models that have inconsistencies considering coherent stratigraphy or have only little evidence for the model. This study presented here provides mainly new data for these attempts.

Geological setting

The southernmost part of the Lepontine Dome structure where the NW – SE to SE-trending cross folds converge into the zone of steep foliation north of the Insubric Fault is a remarkable area: Several nappes are folded in a complicated series of deformation phases. The nappe stack stratigraphy from the Ticino Dome cannot easily be correlated towards the Toce Dome (see Figure 1) and is subject of controversial discussions. The separating structure between Ticino and Tosa Dome is called Maggia Cross Fold or Maggia steep zone (PREISWERK 1921).

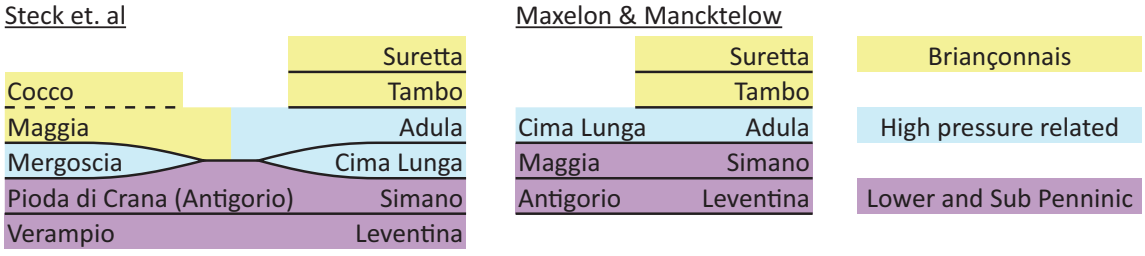

Figure 1 Nappe stack
Attempt to illustrate the nappe stack models with its paleogeograpic origins.

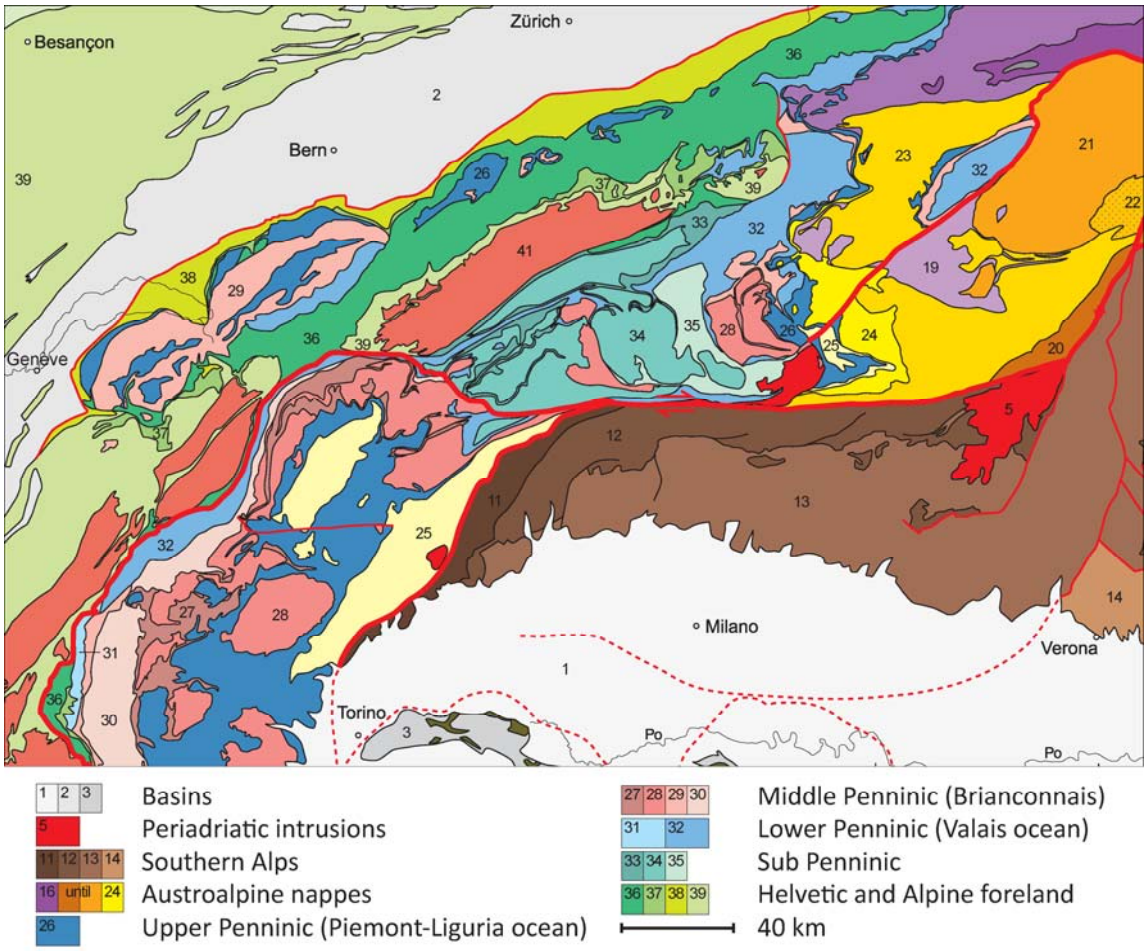

Figure 2 Overview of the central Alpine domains
This study investigates the ductile deformed Sub Penninic domains located between the Insubric Fault in the south (shown here with sense of movement), the Simplon (normal) Fault in the west, the Austroalpine Nappes in the east and the crystalline Aar and Gotthard Massives in the north. This big scale overview shows also the arc shaped form of the Alps. Nappe stack stratigraphy normally follows the rule the further to the south the more internal is the domain and the higher in the nappe in the stack. The term internal refers to the former subduction zone in the south. This simple rule is inapplicable in the Sub Penninic domains because there are cross fold structures. Figure modified after SCHMID et al. (2004).

Metamorphism

The collision of the Adriatic with the European continent and the subsequent subduction of first the Briançonnais slab and then the European margin led to a high pressure metamorphism in the Adula and Cima Lunga Nappes. Adula and probably also Cima Lunga are situated between lower peak pressure metamorphic nappes (FROITZHEIM et al. 2003; STECK 2008). Ultra-high pressure facies was reached for example at the famous Alpe Arami (BURRI 2005; GEBAUER 1996; GEBAUER 1999; NAGEL et al. 2002) within the Cima Lunga Nappe. All nappes underwent later Barrovian metamorphism that increased from the external Helvetic Domain to the internal Penninic Domains. Amphibolite facies starts at the Penninic Front in the north and is cut abruptly at the Insubric Fault in the south (BERGER

et al. 2005). South of it metamorphism is not exhumed due to the missing vertical uplift on this prominent Alpine fault (GANSSER 1968). Immediately north of the Insubric Fault in the Lepontine Dome amphibolite facies was generally reached.

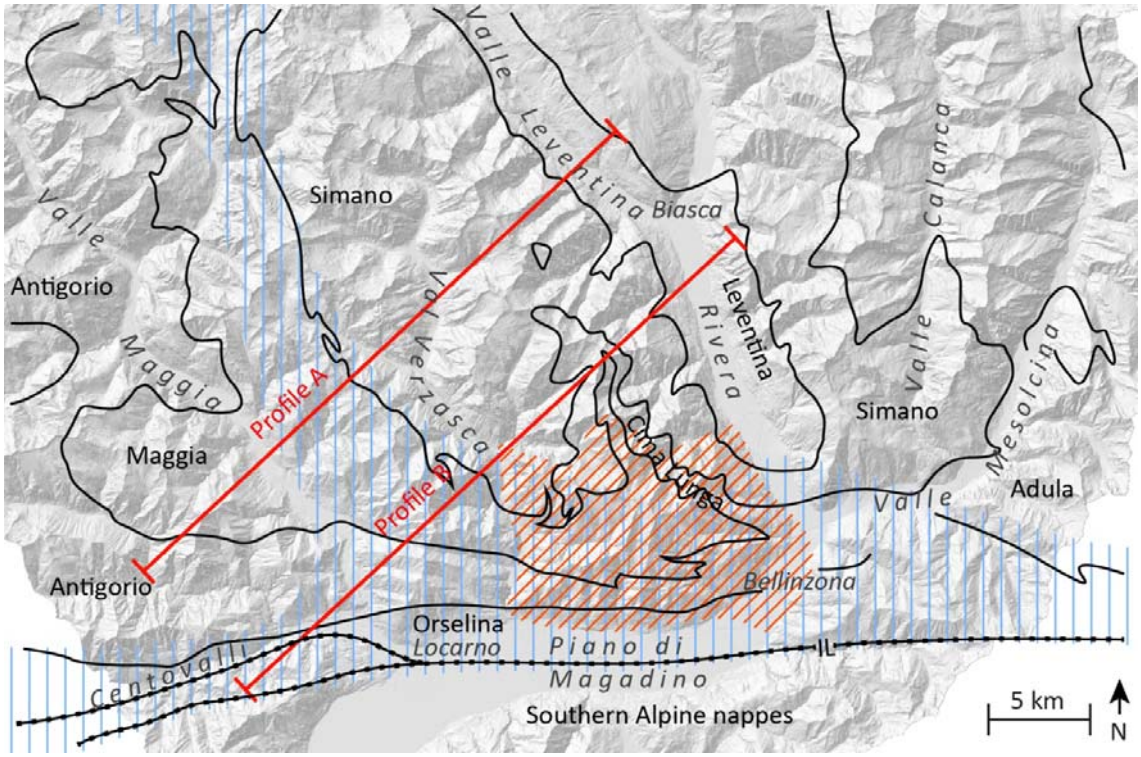

Figure 3 Regional overview of the main tectonic structures
The nappes are drawn after the *Tektonische Karte der Schweiz* (SPICHER et al. 1980; SWISSTOPO 2005). Here the Antigorio Nappe and the Zone of Bellinzona Orselina are separated whereas other authors like Berger et al. (2005) combine these two. Steck et al. (2013) names the eastern part of Antigorio Nappe Mergoscia Unit and Burri (2005) refers to it as Mergoscia-Onsernone Unit.
Diagonally orange hatched the study area between Bellinzona and Valle Verzasca north of the Piano di Magadino.
Vertically blue hatched are the zones with steep dipping foliation (MAXELON and MANCKTELOW 2005). North of the Insubric Fault this is the Southern Steep Belt and between Maggia and Simano Nappe it is called the Maggia Cross Fold.
The Insubric Fault marked with squares on the line is also known as Periadriatic Fault or Lineament. Authors like Gansser (1968) describe the Insubric Fault east of Locarno as the Tonale Fault to be more specific.
Also shown in the figure are the locations of the two cross sections of Figure 5.

High pressure metamorphism is only proven in lenses of different sizes. Together with metasediments and amphibolite lenses they show no obvious geographical pattern. Therefore the lenses of amphibolites and metasediments are considered a tectonic mélange of a tectonic accretion channel TAC by ENGI et al. (2004) and BERGER et al. (2005). However the same map of BERGER et al. (2005) shows that Adula Nappe actually is not a random mélange but has an internal structure. This provides a strong indication that Maggia Nappe and Cima Lunga Nappe have also a tectonic structure, especially since there are also aligned zones of amphibolites and metasediments present. The presence or absence of high pressure relicts or amphibolites can potentially be used to

distinguish different nappes even if the classic metasedimentary nappe separators are absent. BERGER et al. (2005) used this approach for the definition of the Zone of Someo. Note that one should keep in mind that the rocks do not always show their peak metamorphic grade.

Deformation

The Penninic domain in the central Alps shows a complex deformation pattern with several distinct phases (GALLI et al. 2007; GROND et al. 1995; GRUJIC and MANCKTELOW 1996; MAXELON and MANCKTELOW 2005). It deformed mainly in a ductile manner (EPARD and ESCHER 1996). The formation of the nappes caused two north vergent fold phases D_1 and D_2 with almost identical fold axis and flat limbs. During these phases with isoclinal recumbent folds the main foliation was formed. The D_1 phase is preserved in garnet porphyroblasts whereas the D_2 foliation goes around them (GROND et al. 1995). Imbrication of ultrabasic rocks due to thrusting was pre or syn D_1 (GROND et al. 1995). The third deformation D_3 phase has fold axes running north-south that bend to the east towards the Insubric line. D_3 Folds are mainly open except for the Maggia Cross Fold (STECK 1998). These three phases started in the Eocene, strongly overlapped each other and lasted until the Miocene (e.g. timetable of BERGER et al. 2005). After that a transition to brittle deformation took place. The strong uplift north of the Periadriatic Fault described by GANSSER (1968) may be due to slab break off (BLANCKENBURG and DAVIES 1995) and the subsequent gravitational collapse and or back folding of the nappe pile (ESCHER and BEAUMONT 1997) caused south vergent folds and the Southern Steep Belt (MILNES 1974) where folds can even be overturned. Strong shearing was also a consequence of the uplift and the dextral shearing along the Insubric Fault (SCHMID et al. 1987). It should be noted that the deformation history prior to the nappe subduction is largely unknown.

In accordance with GRUJIC and MANCKTELOW (1996), PFIFFNER (1999) and MAXELON and MANCKTELOW (2005) the deformation phases 1 to 5 are adopted in this study (see Figure 4).

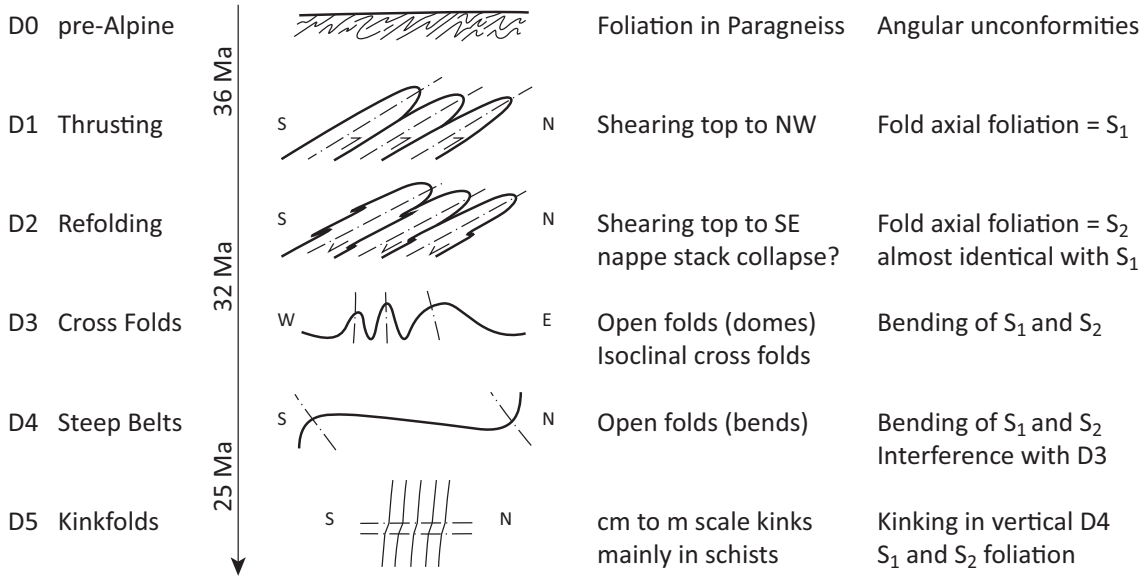

Figure 4 Deformation phases
Dash-dotted lines in the sketch are axial planes of the deformation. Thick lines represent nappe boundaries and thin lines foliations. Not included in the figure is the brittle deformation that followed D5.
Ages on time bar after GEBAUER (1996), GEBAUER (1999) and LIATI et al. (2000)

Ages

Time estimations for the folding phases are given by the early Oligocene age of Alpe Arami high pressure peridotites that predate Alpine deformation phases and the formation of nappes (GEBAUER 1999). Folded leucosomes with an age of about 32 Ma provide a minimum age for the first deformation (GEBAUER 1996). The end of the folding phase east of the study area marks the unfolded Novate granite and dykes in the southern steep belt with an age of 24 to 25 Ma (LIATI et al. 2000). In Lavertezzo little deformed aplite dykes with an age of 20 Ma crosscut the folding structures and mark their minimum age (ROMER et al. 1996). These dykes still show slightly oriented mica that conserved the decreasing north south compression stress situation. Dating of the Cocco units in the upper Valle Maggia give a Carboniferous age of 300-310 Ma (BUSSIEN et al. 2011).

Petrology

The petrology of the study area is dominated by different types of gneisses. There are non continuous amphibolite layers, rare metacarbonate and marble lenses and few mafic and ultramafic lenses like Alpe Bardughè and Alpe Arami. The overall petrology of the nappes is very similar. The gneisses are highly heterogeneous due to isoclinal folding or pre-Alpine folding. The vast majority of these inhomogeneous gneisses are plagioclase feldspar augen-gneisses (BÄCHLIN et al. 1974). There are leucocratic albite oligoclase microcline gneisses mainly in the Alpe Ruscada and Valle della Porta area. Paragneisses are present in the Gaggio and Madone area and also at Alpe Bedretto on the path to Alpe Arami. Furthermore there is the very distinct recognisable Cocco Gneiss (due to biotite nests) that is sometimes associated to an intrusion with a complex history (WENK 1982). It is very similar to the Matorello Granodiorite in the Sambucco Lobe (BUSSIEN et al. 2011). The partial melting in the south is according to RUBATTO et al. (2009) due to influx of fluids.

Nappes

- Maggia Nappe contains leucocratic albite gneiss with now gneissic Cocco diorite and Ruscada leucogranite that intruded in the Palaeozoic (BUSSIEN et al. 2011).
- Cima Lunga Nappe is a heterogeneous assemblage of orthogneiss and paragneiss with amphibolite, mafic and ultramafic lenses and metacarbonate layers (BERGER et al. 2005). The metamorphic peak conditions range at least from amphibolite to eclogite facies.
- Simano Nappe is in the southern part dominated by leucocratic two-mica-gneiss called Verzasca Gneiss (BÄCHLIN et al. 1974). The northern part of Simano Nappe differs from the south and is treated as a separate map by authors like Steck et al. (2013).
- Leventina Nappe is separated by Simano Nappe by quartzite and metasediments but has a similar leucocratic two-mica-gneiss composition (BERGER et al. 2005). A mylonite band is a further criterion for the separation in the southern parts of the nappe (RÜTTI et al. 2005).
- Antigorio Nappe or Mergoscia Unit is formed by inhomogeneous leucocratic gneiss (BÄCHLIN et al. 1974). Where it contains lenses of amphibolite and metacarbonate it is referred as Mergoscia Unit by STECK et al. (2013) and listed together with Cima Lunga and Isorno-Orselina.
- Orselina Unit is comparable with the Cima Lunga Nappe but contains no high pressure metamorphic rocks (STECK et al. 2013).

Authors like ENGI et al. (2004) radically unite all nappes that contain lenses to a tectonic mélange or tectonic accretion channel (TAC) and refer to Cima Lunga, Orselina or Mergoscia only as subunits.

Previous work

Geological maps and surveys

With the *Geologischer Atlas der Schweiz Blatt 1313 Bellinzona* a precise map is available. BÄCHLIN et al. (1974) included also older field observation from GANSSER (1968), WENK (1955) and PREISWERK (1921) in this map. Recently only few field work was done directly in the study area. An exception is the petrological study of BURRI (2005) that assessed the metamorphic facies. Adjacent in the north in the Cima di Gagnone area (Cima Lunga Nappe) master projects studied the petrology and made detailed maps. About the same region PFIFFNER (1999) published a PhD thesis that contains interesting thoughts about the Valais trough origin of the ophiolites found in the Cima Lunga Nappe.

Tectonic models

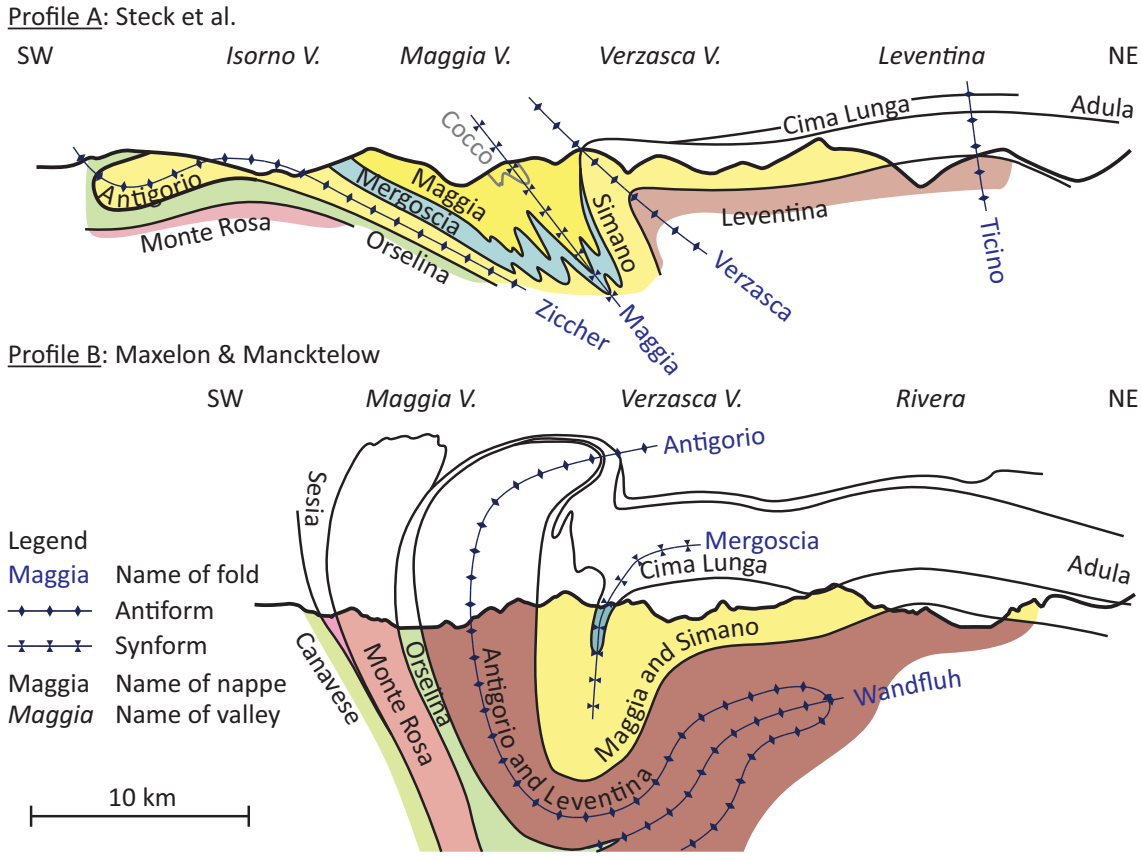

Figure 5 Comparison of two profiles through the same structure
The interpretation of the Maggia Cross Fold after STECK et al. (2013) on profile A and the interpretation of the Southern Steep Belt after MAXELON and MANCKTELOW (2005) on profile B are incompatible because nappe stratigraphy differs completely. Both profiles are simplified after the authors. Profile B is mirrored in order to have identical orientation. The profiles are parallel and separated by only 8 km in strike direction. The geographical location of the profiles is shown with red lines in Figure 3. For the sake of the distance major differences are very unlikely.
The study area begins 7 km south east of the centre of profile B.

The main discrepancy in the large scale interpretation is the position of the Maggia Nappe (see Figure 5). Authors like STECK et al. (2013) or BERGER et al. (2005) show in their sections and interpretations that the Maggia Nappe lies on the Cima Lunga Nappe. This implies Cima Lunga to be connected to the Mergoscia Nappe (or Antigorio Nappe respectively). MERLE and LE GAL (1988) (and MERLE et al. 1989) share this view of west vergent cross folds due to sub domes and point out that below both Simano and Antigorio a mylonite zone with top to the west movement was observed. But this can also fit for other models such as the one from MAXELON and MANCKTELOW (2005) which presents a section that shows Maggia and Simano Nappe as one nappe. According to this interpretation the Cima Lunga Nappe is the core of the Mergoscia Synform. As a consequence the Leventina Nappe is then correlated to the Antigorio Nappe. Further evidence for this model is found in the discussion of GROND et al. (1995) where the Cima Lunga Nappe is interpreted as a western closing fold.

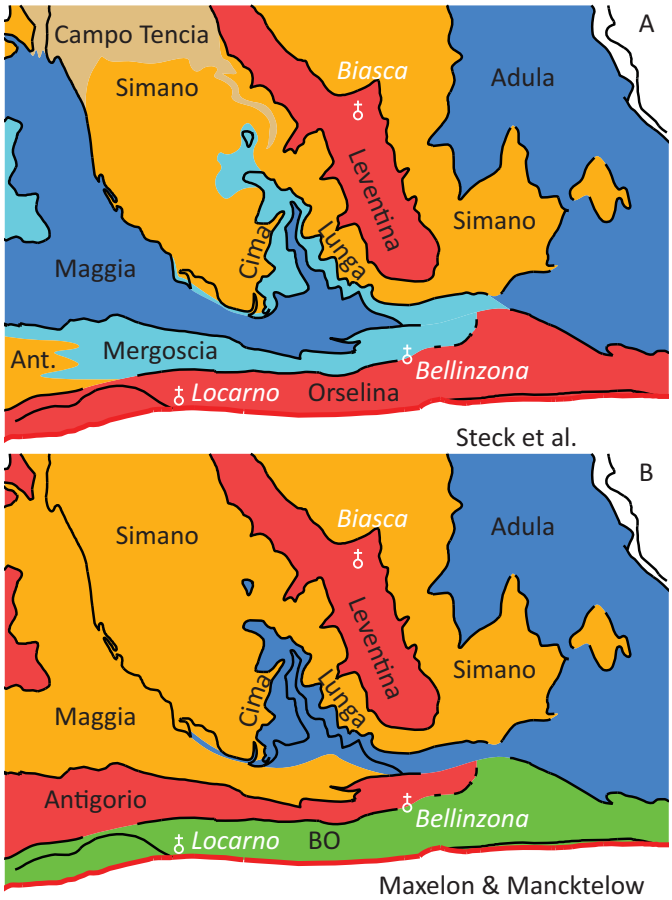

Figure 6 Nappe correlation
Simplified visualisation of the different nappe interpretations. Black nappe borders after the *Tektonische Karte* (SPICHER et al. 1980). Colours show nappe interpretations after the authors.
A: After STECK et al. (2013) Simano and Antigorio are equivalent.
B: After MAXELON and MANCKTELOW (2005) Simano and Maggia Nappe are equivalent and Cima Lunga lies above.
Compare with the nappe stack (Figure 1) and the cross sections (Figure 5).

Research goals

The basic questions are raised by MAXELON and MANCKTELOW (2005) or BERGER et al. (2005) where they list some main unresolved problems in the Lepontine dome: The tectonic position of the Maggia Nappe in reference to Simano Nappe as shown in Figures 3, 5 and 7. And the assumed antiform north of the Insubric Fault that contradicts the vergences of the observed parasitic folds on outcrops.

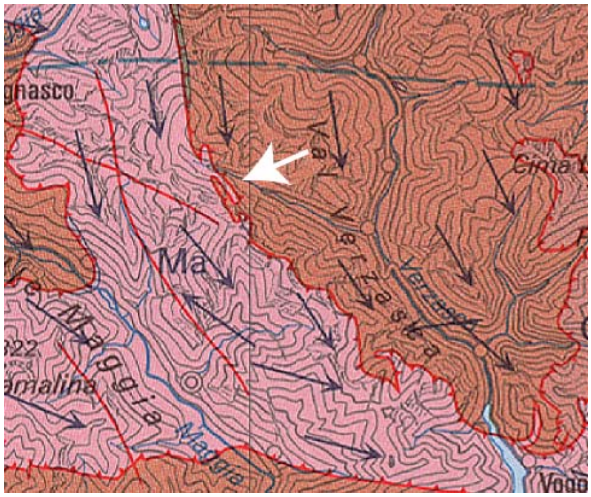

Figure 7 Detail of the *Tektonische Karte der Schweiz*
The arrow points towards the nappe boundary between Simano Nappe and Maggia Nappe in the Maggia Cross Fold where the teeth indicating way up change direction. This is an obvious stratigraphic problem of the nappe stack.
The stratigraphy in the north is based on Mesozoic sediments whereas in the south no unique observation provides a clear nappe relation. Scale of the map is 1:250'000. Modified after SPICHER et al. (1980)

On the tectonic map of Switzerland by SPICHER et al. (1980) (see Figure 3 and 7) there are difficulties to correlate the nappes north-east and south-west of the Maggia Nappe due to the Maggia Cross Fault. What is named Antigorio Nappe on the tectonic map contains in some parts relicts of high pressure metamorphism and therefore BURRI (2005) calls this part Mergoscia-Onsernone Nappe. Generally the nappe definitions in the southern Lepontine cause problems because the classical sedimentary nappe separators are missing and replaced by a not equivalent core and cover concept or other lithological approaches (WENK 1953). This could for example be seen at the unclear boundary definition between Simano Nappe and Maggia Nappe. On the map a switch of the arrows on the nappe boundary (see Figure 7) eludes the problem. This specific problem is often solved by the introduction of the Campo Tencia Nappe (e.g. recently done by STECK et al. 2013). But elsewhere the situation is dubious as well: North of Bellinzona (see Figure 3) the Antigorio, Cima Lunga and Adula Nappes have no clear separation. The map could avoid a clear statement below Quaternary cover.

Three dimensional (3D) models of the study area are a result of the work. To create the models lithological observations were required to define reasonable stratigraphy that is needed as basic assumption for the model. Therefore the geological map sheet Bellinzona by BÄCHLIN et al. (1974) was mainly used but also new lithologic analysis with samples and thin sections were done to evaluate and improve the knowledge displayed in the map. The main aim of rock sampling was to potentially differentiate metasediments and amphibolites that are widespread and also to assess the sense of shear to develop a combined kinematic and geometric model of the region.

A new idea interpreting the genesis of the cross faults and is also a result of this study.

Methodology

Field work

Observing and measuring structures was essential and a key part of the work for this thesis. Substantial time was invested to do observations in the field. The field survey comprised a search for outcrops that show as much combined structural elements as possible to get an idea of the relations of the structures.

At the outcrop, structural measurements of foliations, lineations, fold axis, fold axial planes, joints, slickenslides and veins were done. Photos and sketches were used to identify the relations of the structural elements and the style of folding. Observations of parasitic folding were done to have an idea of the vergences at the outcrop scale and to constrain the large scale fold geometry.

The lithology of the outcrops was noted and compared with the geological map of Bellinzona from BÄCHLIN et al. (1974). Special attention was given to the degree of migmatization of the rock and the relationships of different fold structures such as cross-cutting structures.

Both lithology and structures were studied on characteristic rock samples that were oriented and collected during field work.

Processing and analysing

GIS

All spatial information and measurements were managed with ArcGIS from ESRI. All outcrops have a point feature in the database that was spatially placed after the field map. The point data were completed with notes from the field book. The following attributes were managed in a table:

- Unique outcrop point number
- Height measured with a pressure altimeter
- Observed lithology
- List with the numbers of the samples of this outcrop
- Notes about photos
- Observations in which direction the antiform is closing
- Notes about migmatization
- Calculated east and north coordinates (CH 1903)

All measurement data were handled with a second table. This table is connected with the outcrop table by the unique outcrop point number. This table contains the following information:

- Unique outcrop point number
- What type the measurement is (S for planes, L for linears, D for ductile, B for brittle)
- Azimuth angle
- Dip angle
- Further information about the measurements

The table of outcrops and a connected table with the measurements were the basis for spatial query of the data (to define polygons) and its exportation into stereoplot software. With ArcGIS maps showing the data were done. They were used to define areas with similar foliation data. Then polygon features for areas with similar foliation orientation were defined.

Stereoplots

Within the areas with similar foliation stereoplots that show schistosity, lineations and fold axis were made to analyse the structures. Stereonet (scientific algorithms to this program are described in ALLMENDINGER et al. 2012), OpenStereo (open source project of GROHMANN and CAMPANHA 2010) and TectonicsFP (REITER and ACS 1996) were used for this task. The latter was also used to model the stress situation (detailed description by ORTNER et al. 2002). All generated stereoplots show equal area projections (or Lambert azimuthal projection) into the lower hemisphere.

Maps and profiles

A verification of the lithology of the geological map of BÄCHLIN et al. (1974) was done with GIS outcrop data overlain onto the map to compare it with field observations. The spreading of migmatization within the southern steep belt was also displayed in this map (see appendix: Lithology and migmatisation).

All other data were used to create separate maps that show the orientation data of foliation, lineations, folds and faults as well as the observed vergences of the folds. There is also a map that shows what was observable on each outcrop (see appendix: Field observations).

Field data were incorporated in a set of north-south and west-east profiles that were drawn with Illustrator to do a manual interpretation of the nappe system.

3D Model

GeoModeller software

Intrepid GeoModeller is a software developed by BRGM, France (*Bureau de Recherches Géologiques et Minières*) that is now further developed by Intrepid Geophisics in Australia (MCINERNEY et al. 2005).

As described by CHILÈS et al. (2004) and MCINERNEY et al. (2005) GeoModeller uses the potential field theory and assumes every contact as an isopotential surface. The contacts are provided as points with three dimensions. All points of the same contact have no change in potential. The field orientation data (dip and dip direction) are interpreted as gradients in the potential field. The dip is always orthogonal to the isopotential line. Since every potential field must have a direction vector a stratigraphic column has to be defined that provides an order for the contacts. Every formation or group of formations must have a clear extent with its own potential field. Since this field represents a geological object it is defined by a common deposition and or deformation history. A contact has either eroded into older units or is onlapping on them. This information has to be provided to GeoModeller. Faults are also handled as borders for isolines.

Information about the deformation such as fold axial plane or fold hinge can also be included in the model. The weight of this information seems to be so low, that the model did not respond much on these input data in this study. The input of the angle between fold limbs in order to model isoclinal folds did as well not influence the model much.

A big advantage of the potential field method of GeoModeller is that orientation data can be entered at any place in the model not just on the contact and, on the contrary, a contact can be inputted without orientation data. This is very significant in this study because there are no clear contacts but a lot of orientation measurements.

Model hypothesises

To create the model the following assumptions and simplifications had to be made:

1. GeoModeller is designed to use stratigraphic layers as contact data. In this study the rocks have no visible primary layering or bedding and are strongly deformed so that they lost their clear bedding information. Therefore nappe boundaries are used as units in the tectonic pile even though these boundaries are likewise not well defined. Contacts follow the foliation plane of the nappe boundary. It has to be noted that this definition fails if the primary deformation foliation is completely overprinted by later deformation.
2. All nappes are considered to have the same history after their emplacement. Thus they are handled as a stratigraphic succession. The model input contact parameter is onlap within the succession. Since some nappe boundaries show more shearing than others this simplification has to be kept in mind as a possible source of errors. Such a contact between Leventina and Simano Nappe is described by MERLE et al. (1989).
3. The petrological survey done by BÄCHLIN et al. (1974) for the geological map are assumed to be basically correct. Hence it was used in the model to fill the gaps between own petrological observations.
4. The stratigraphy is an object of the study and hence unknown. Nevertheless it has to be defined before models can be calculated. The interpretation of STECK et al. (2013) (referred to as A) and the interpretation of MAXELON and MANCKTELOW (2005) (referred to as B) were used as base for the models. As explained in the introduction the difference lies in the nappe correlation. In the model this specifies what is considered as the same nappe in the model: Either Antigorio and Simano Nappe are considered associated or Maggia Nappe and Simano Nappe are modelled as the same unit.

Input basic data

The project was set up with Swiss national grid coordinates CH1903. The processing extent was defined with:

X	707’500 ≤ X ≤ 725’000	17.5 km
Y	111’000 ≤ Y ≤ 130’000	19.0 km
Z	-5’000 ≤ Z ≤ 7’000	12.0 km

Digital elevation data from SWISSTOPO (2001) was imported to create the surface section. The used digital height model DHM25 has a spatial resolution of 25 m and a vertical precision of 2 m in valleys and 8 m for higher elevations. On this surface the topographic maps Osogna from SWISSTOPO (2008a) and Bellinzona from SWISSTOPO (2008b) were overlain. Data entered in 2D was automatically given the elevation of the surface section as third coordinate. The geological map (BÄCHLIN et al. 1974) was imported on this surface to digitise the contact data.

Input field observations

All input parameters are point parameters. The lines (e.g. on Figure 8) serve only as an optical help to recognise the border of the contact points. At least one border point from every formation has to be defined. The contacts are shown as footwall borders. This means that the shown border is always the lower limit of the nappe. The upper border is given by the border of the next higher nappe in the stratigraphic column. Contacts are in the form of foliation planes that serve as fictive nappe separators. The orientation data comes from field measurements. The allotment to a nappe was done on the geological map in GeoModeller. Each orientation point was given the attribute normal

or overturned stratigraphy corresponding to its location and the corresponding model. This way up attribute has a major influence on the result and can even make the computation impossible.

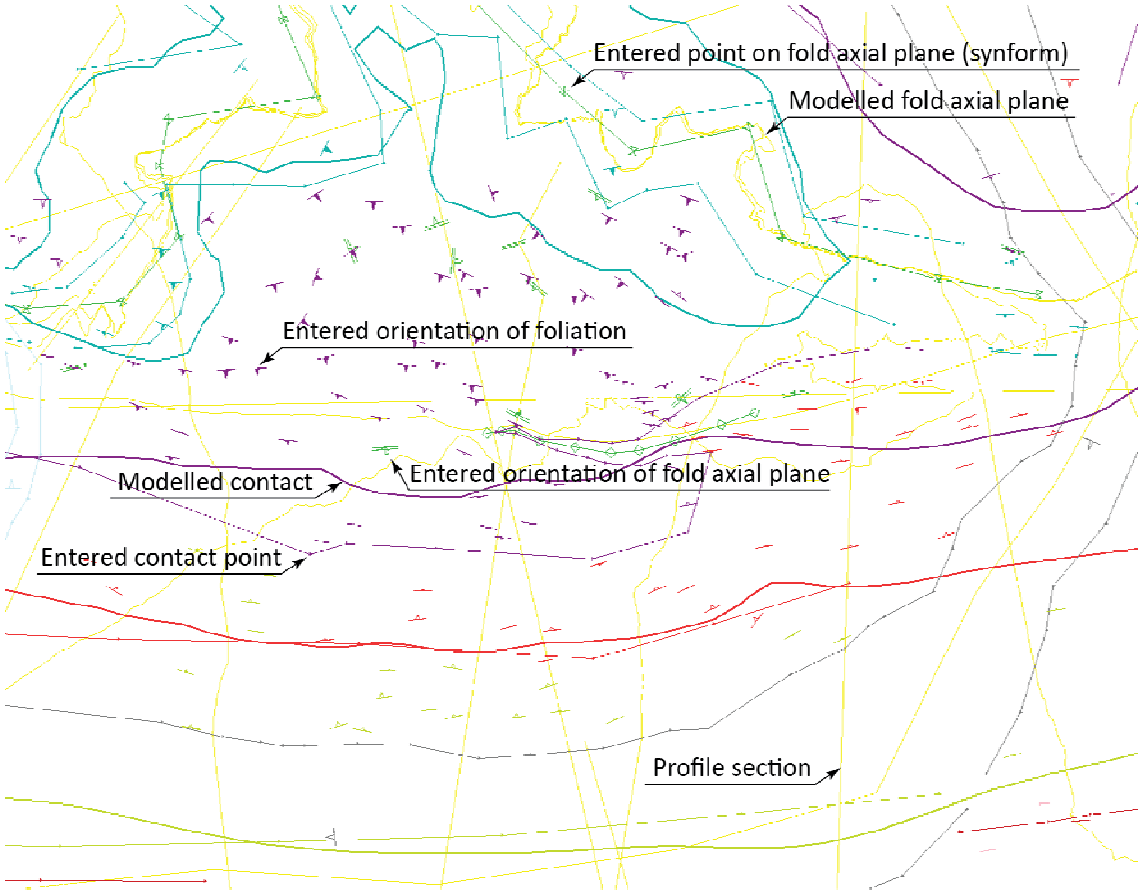

Figure 8 Screenshot of all input parameters on the surface section
The colours refer to the different units defined in the stratigraphic pile of model B (see Figure 27). The thin lines indicate the input geometry and the thick lines the output geometry. Shown in yellow are profile sections. All deformation data such as fold axial plane or axial plane trace are shown in green.

Modelling parameters

The model interpolation parameters do have a very strong influence on the result of the model and its similarity to field observations. These parameters define how strong the influence of a single measurement is in order to avoid conflicts of points that are too close or have dissimilar values. The range of influence that a point can have in the first place was limited to 10 km. The geostatistical nugget effect on geology data is modelled with 10^{8}, geology orientation data value is 0.1 and drift degree is 2. The mathematical background is described by CHILÈS et al. (2004). Best practice values are the default values (COURRIOUX personal communication 2014; CAMPANI personal communication 2014): Geology data with 10^{-6} and geology orientation data with 0.01. First models were run with these parameters but they did not work for this study because they cause an error in calculating the model. Wrong parameters can also lead to a layer cake model. The parameters for every series of formations can be edited individually.

Results

Petrologic survey

Orthogneiss

This leucocratic two mica albite gneiss appears as fine grained streaky or coarse grained augen gneiss. It contains no alumosilicates. The rock is named Ruscada Gneiss in the study area and is already mentioned by PREISWERK et al. (1918). This name does not refer to the Pizzo di Ruscada (SPICHER et al. 1980) but to the northern part of the Alpe di Ruscada. The Ruscada Gneiss is associated with the Maggia Nappe.

Often the gneisses are inhomogeneous and contain lenses of amphibolites and calcite silicates. Leucocratic veins and migmatites are often observed.

Cocco Gneiss

This rock type is one of the rare examples of clearly distinguishable petrology in the study area. It was also already described by PREISWERK (1931). He pointed out that the dykes that intruded the country rocks make petrologic partition after deformation even more complicated. It contains typical biotitic aggregates that are embedded in a deformed granodiorite. The Cocco Gneiss is usually enveloped by Ruscada Gneiss and therefore associated with the core of the nappe.

Paragneiss

It is a mesocratic mica-rich gneiss sometimes also fine grained schist. Garnet and alumosilicates are often only visible in thin sections. Kyanite is present and small amounts are retrograde transformed into sillimanite due to decreasing pressure. Paragneiss is associated with the borders of the nappes.

Amphibolite

The different amphibolite lenses consist of plagioclase, hornblende, biotite and pyroxene. Some samples are very rich in mafics. Garnet was only sparsely observed in amphibolites. It is unclear what the peak metamorphic conditions of the amphibolites were and if these metamorphic peak conditions were identical in the study area. Amphibolites are found in all nappes except for the Cocco Gneiss. The ultramafic rocks often occur at the same tectonic position as amphibolites.

Eclogite

Eclogites with the classical garnet and omphacite composition were found around Alpe Arami and on the way there at a small road outcrop above Gorduno. The change into amphibolites is observable.

Mafics and Ultramafics

On Alpe Arami a famous outcrop with garnet eclogites is found as a rather big lens. On Alpe Bardughè a mafic lens in a grassy alp contains enstatite and rodingites. Ultramafic blocks of unknown origin were found north of Alpe Gariss. SPICHER et al. (1980) describes further outcrops in the Valle della Porta at Corte di Fondo, south-west of Monti di Ditto and others south-east of Bellinzona that were not inspected.

Metasediments

What is summed up in the geological atlas as marbles due to the smallness of the lenses can be differentiated at a small scale in a brownish coarse grained silica calcite marble that reacts strong

with HCl and one that reacts less with HCl and contains visible actinolite. Under the microscope there was also scapolite visible in the latter rocks.

Aplite

Granitic pegmatitic dykes are very common in the study area. On Pianca south of Madone they form dykes traceable for several hundred meters. The pegmatites contain feldspars, plagioclase, quartz and mica. Tourmaline was only twice observed as macroscopic crystals. At Alpe Albagno (right behind the hut) they form idiomorphic crystals up to 5 cm in diameter. The aplite is oriented with the foliation (185/50) and almost pegmatitic appearance. SE of Mornera up to 5 cm large magnetite crystals were found in a leucocratic aplite that was also oriented with the foliation (332/42).

Pegmatite

On Pianca there are aplites that differ from the pegmatites only by the increased crystal size and muscovite content. The pegmatites are not deformed and cut the country rock discordantly. They are vertical and strike N-S around 200°.

Migmatites

Local melting was observed in the whole study area (see appendix: Lithology and migmatites). Leucocratic melts are surrounded by melanocratic restites. Most migmatites are deformed.

Rock samples

The rock samples were cut in (mostly orientated) 30 µm thin section. The main attention was laid on microstructures such as sense of shear and on special features that can be used to differentiate lithologies better than done on the available maps. Sense of shear is only well visible in quartz veins but almost no sample provides good quartz veins to observe preferred orientation of quartz.

Sample 1: Outcrop 4, way from Gnosca to Mondella

The sample is from a quartz vein that is orientated with a foliation 164/56. It lies in the Simano Nappe. Figure 9 shows a photomicrograph with a clear sense of shear that indicates a top to the south movement. Undulose extinction indicates deformation during decreasing temperatures above 500°C in amphibolite facies.

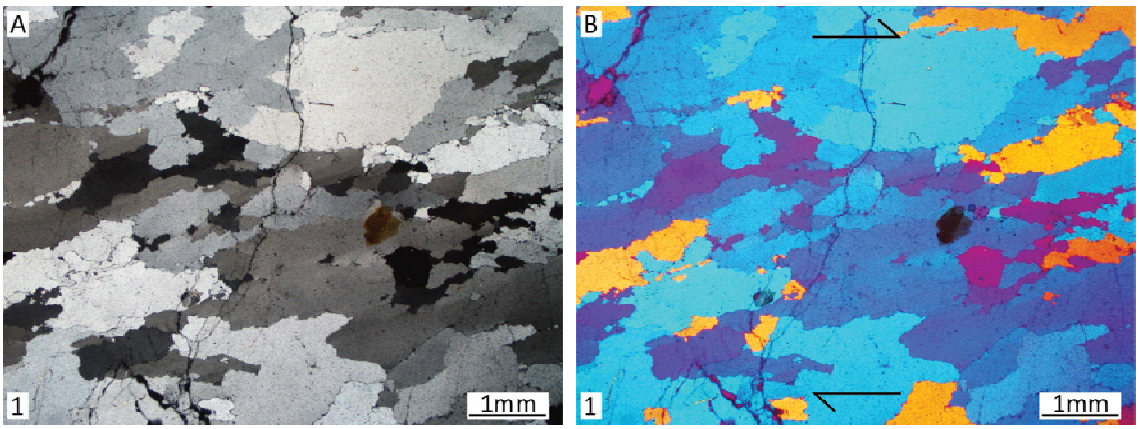

Figure 9 Photomicrographs of sample 1
Thin section cut parallel to lineation. Photo A was made with crossed polarised light and B with additional lambda plate. Quartz shows undolose extinction and grain boundary migration. Using lambda plate a preferred orientation of the c axes is visible which proves a top to the south shearing at this outcrop.

Sample 2: Outcrop 6, way from Gnosca to Mondella

The sample has a foliation orientated 237/47 and a second foliation oriented 158/65 and lies in the Simano Nappe. The sample was taken from a peraluminous (garnet containing) dyke and reacted with acid. Quartz veins could not develop equilibrated recrystallized grain boundaries with 120° triple points due to fast ex-humation and cooling. Grain boundary migration at amphibolite facies is still visible (see Figure 10).

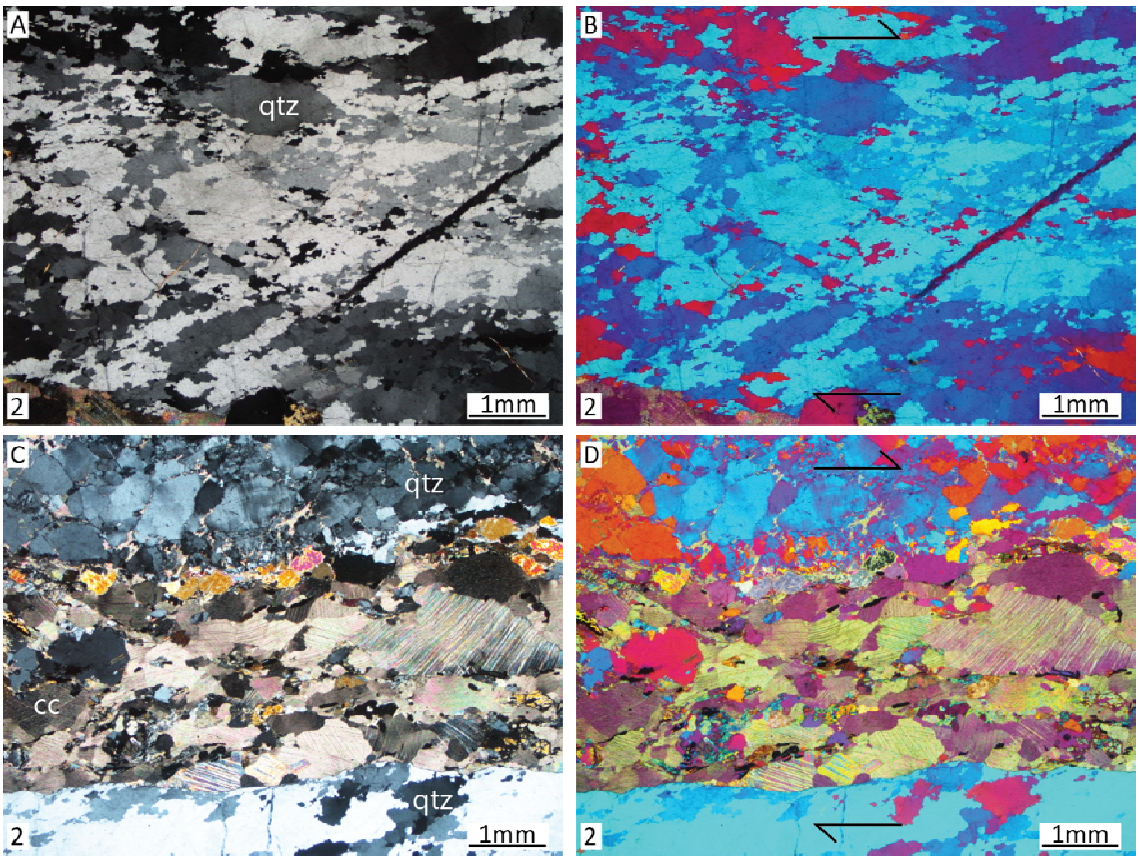

Figure 10 Photomicrographs of sample 2
Thin section cut parallel to lineation. Photo A and C were made with crossed polarised light, B and D with additional lambda plate. In quartz a preferred orientation of the c axes is visible indicating a dextral sense of shear in the section and a top to the south shearing on the outcrop. Both places show filled cracks or veins, in A and B the fill is quartz. In C and D it is calcite and probably small amounts of diopside and epidote.

Sample 2a: Outcrop 20, Alpe Albagno

This sample shows a folded paragneiss (fold axis 252/31). The fold belongs to D1 and was refolded by D2. With a hand lens fibrolitic sillimanite was visible. In the thin section (see Figure 11) mica consumes kyanite. Both suggest a retrograde trend of high to low pressure.

Sample 8: Outcrop 45, Ör della Meda, Maggia Nappe

The sample has a foliation plane of 197/52 and a fold axis of 288/10 and a fold axial plane of 202/35. The sense of shear is top to the north east. The paragneiss is crenulated with a top to the north shearing. The paragneiss contains garnet and alumosilicates.

Sample 10: Outcrop 38, Capanna Albagno

Up to 5 cm large tourmaline are found in this dyke (185/50). Outcrop 193 near Alpe Ruscada shows similar tourmalines as this sample. Abundant myrmekite is observed in this sample. Myrmekite indicates the high pressure side of the clasts (SIMPSON and WINTSCH 1989).

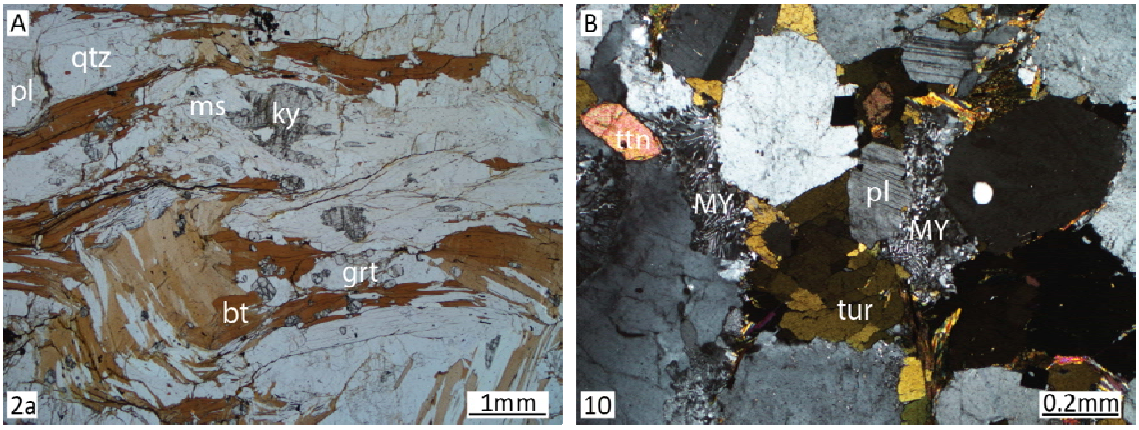

Figure 11 Photomicrographs of sample 2a and 10
Picture A (sample 2a) is cut perpendicular to the fold axis. B (sample 10) is a crossed polarised light photo. MY points towards myrmekite.

Sample 12: Outcrop 162, Above Monti Bassi (Sementina)

Sample was taken from a small location with different calcite marbles and calc-silicate rocks. The sample suffered from little deformation and is recrystallized. This indicates high temperatures outlasting deformation phases. The hand sample reacted a little with acid even though there is no visible calcite. Foliation plane is 340/67.

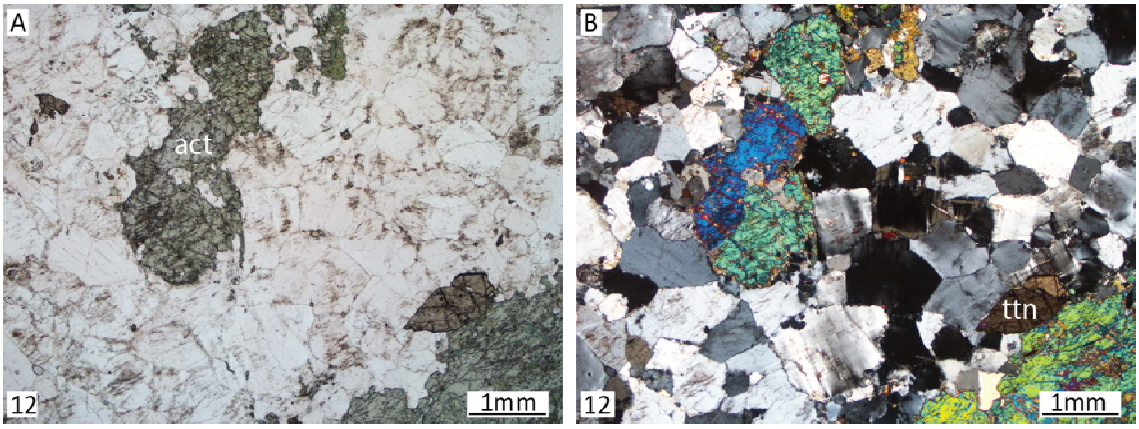

Figure 12 Photomicrographs of sample 12
Photo B is taken with crossed polarised light. The thin section shows amphibole (actinolite and tremolite?).

Sample 13: Outcrop 236, SW of Mornera

The sample was taken from a poorly exposed outcrop because there are magnetites up to 5 cm in size in a leucocratic aplite. BURRI et al. (2005) are the only authors that mention the magnetites without interpretation. The sample also has myrmekite structures that indicate high pressure (SIMPSON and WINTSCH 1989).

Sample VO1 and VO2: Outcrop 520, Alpe Bardughè (Vogorno)

Samples are taken from the mafic lens SW of Alpe Bardugè. Observations indicate a metarodingite occurrence on this outcrop. As shown in Figure 13 in VO1 olivine, amphibolite and ilmenite were observed. In sample VO2 a blackwall of olivine and enstatite is an indication on a metarodingite.

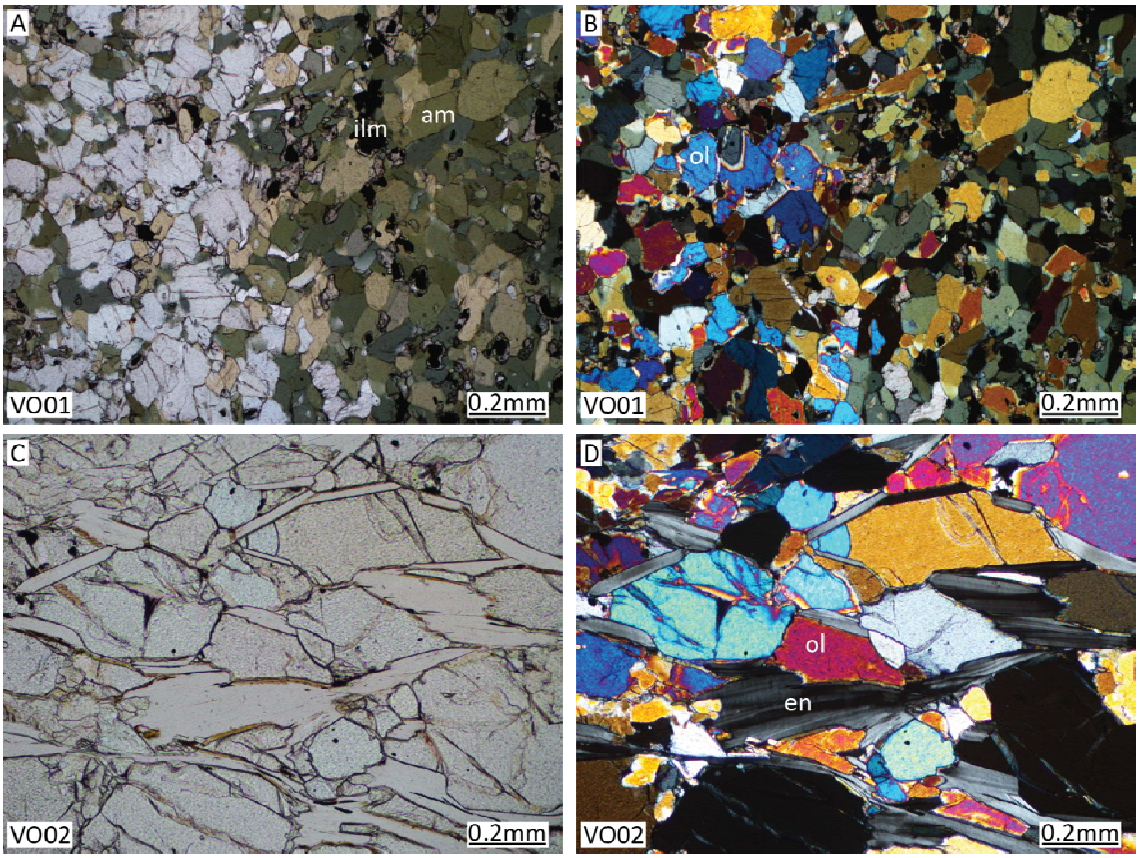

Figure 13 Photomicrographs of samples VO01 and VO02
Both samples are not oriented. Both contain olivine. The amphibole in A and B is mainly hornblende.

Foliation

Foliation is formed by a schistosity of syn-tectonic metamorphic grown biotite and muscovite and flattening and or orientation of pre-existing minerals such as biotite (especially in Cocco Gneiss) or feldspars. Often the foliation is also accented by shearing on the same plane.

Foliation shows a trend from flat (0-10°) in the north to steep or even overturned in the south. From west to east the dip turns from SSW to SSE in the steep and overturned zone. Note that the term overturned refers here to field observations. Applying the nappe model from MAXELON and MANCKTELOW (2005) some measurements considered overturned are in fact normal lying. Besides the main foliation there is also a second foliation which has a roughly 20° steeper dip but the same azimuth. This second foliation bends as well but it is better visible in the north than in the south of the field area. Differentiation between S_1, S_2 or even further foliations was only possible if several foliation planes were exposed on the outcrop at once. Assignment a single measurement to a foliation generation is ambiguous because dip and azimuth values are all very similar. The calculated map of the S_1 dips in Figure 14 potentially contains foliation that belongs to other generations.

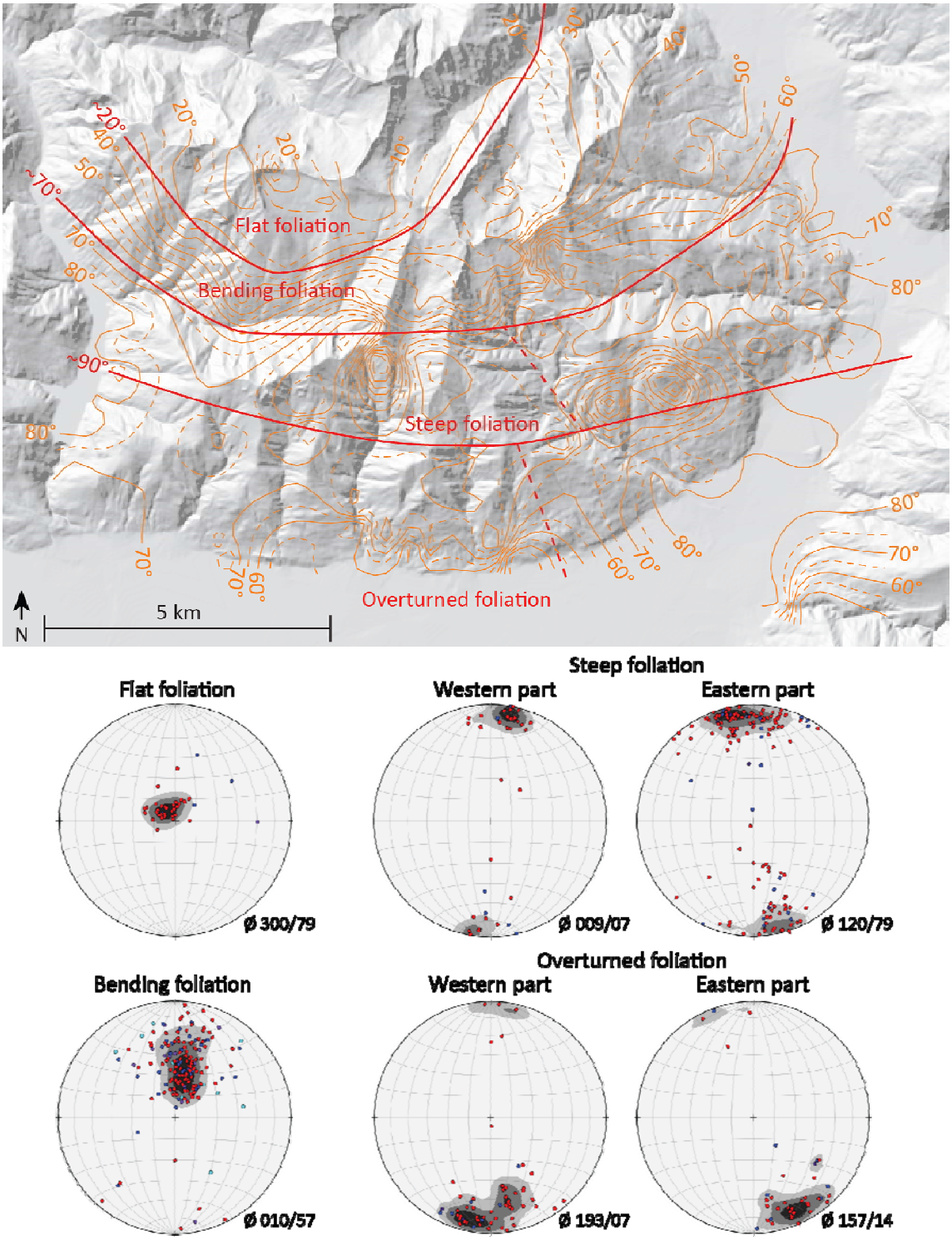

Figure 14 Map view and stereographic projections of the foliation data.
The map shows in orange calculated contour lines of the dip angles of main foliation S_1. Azimuth data was not used for this calculation. Red lines show the manual simplification of the calculation that was used to define areas for the stereoplots below.
The stereoplots show with red dots foliation S_1, in blue foliation S_2 and in violet and light blue dots all further foliations. The grey scale shows the point density.

Linear fabrics

Two kinds of lineations were observed: Intersection lineations and mineral lineations. Both are parallel to the fold axes in the same region. Intersection lineations are best visible on foliation forming minerals as biotite. There is a smooth transition to crenulations. Mineral lineations are mostly formed by mica (biotite) and quartz. Most of the observed linear fabrics are a mixture of intersection and mineral lineation. Since discrimination of the two types of lineations is vague and orientations are similar they are not analysed separately.

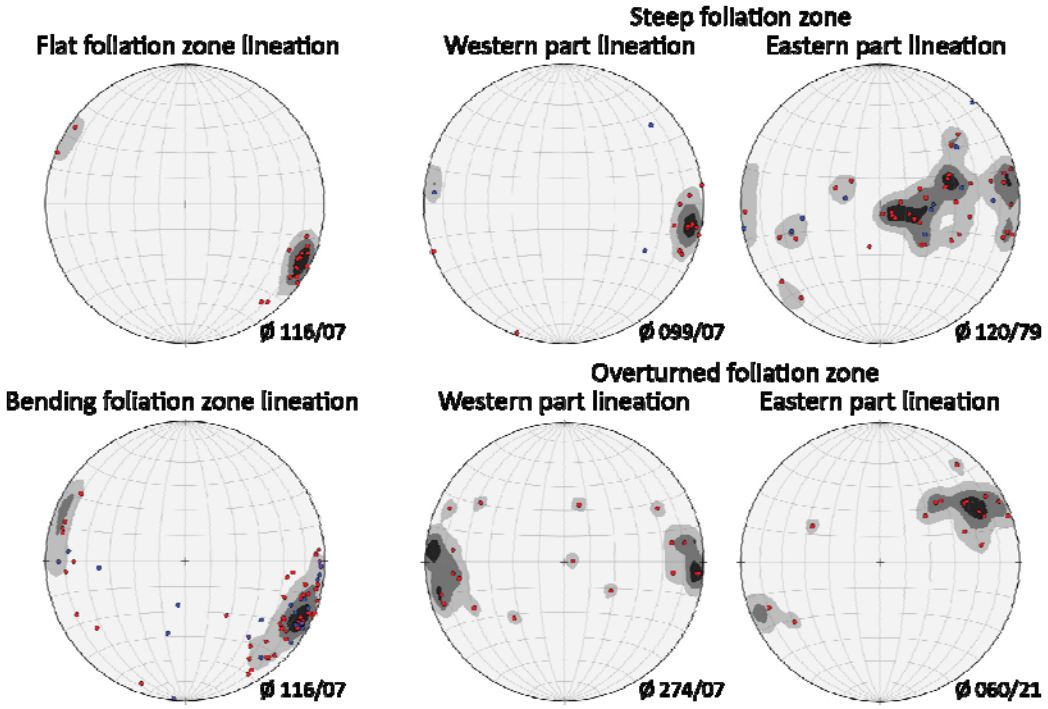

Figure 15 Stereoplots of the lineations
The plots use same spatial division as in Figure 14. Red points show first lineation L_1 and blue point show second lineation L_2. The grey scale shows point density. The figure shows intersection and mineral lineations combined.

There are relations between the different lineations as documented in Figure 16. The used indices L_1 are always referring to the east dipping lineation. These two discriminable lineations are also visible in the stereoplots in Figure 16 (bending foliation zone and eastern part steep zone).

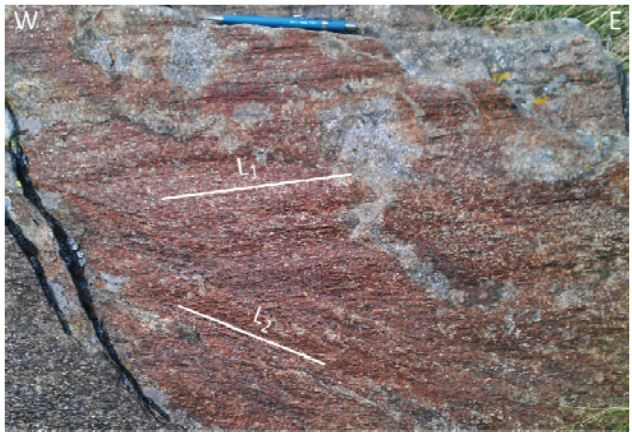

Figure 16 Photo of lineations
Outcrop 133 is only 500 m east of Alpe Albagno in the eastern part of the bending foliation zone. Two different clear lineations L_1 290/03 and L_2 120/20 are visible. Both are a combination of mineral intersection and crenulation intersection.
Foliation is 223/70. On the photo L_1 is overprinting L_2 at the outcrop itself this relationship was not that clear.

Shearing

Sense of shear indicators were assessed on rotated clasts (sigma or delta clasts). The sense of shear was also visible in some thin sections (see Figure 10). Since almost no quartz is present in veins we got only two samples that show a clear preferred orientation of quartz in thin sections.

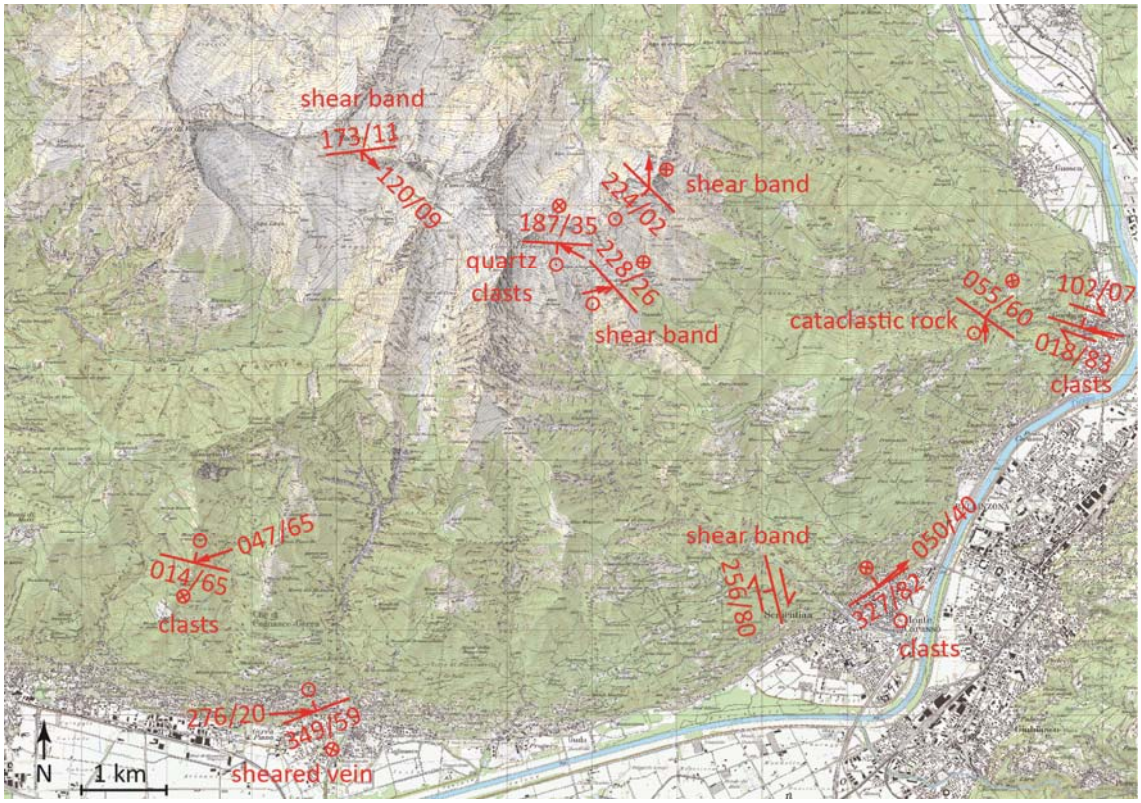

Figure 17 Sense of shear observations
The overview combines 10 measurements of 14 outcrops. Orientation data is for shear plane and lineation (if available).

Folding

Fold style and vergences

Figure 18 Fold styles
The deformation phases created fold patterns that can be discriminated based on their style. D1 and D2 are associated with isoclinal folds. The more open folds of D3 and D4 overprinted and deformed the D1 and D2 foliation. D5 caused kink folds.

There are basically two main fold styles that can be differentiated: Folds with almost isoclinal spiky folds that form a new axial plane foliation and a second group that has more open folds with M-style parasitic folding in the hinge zone. Parasitic D2 folding structures show predominant antiform to the south vergences (see map appendix: Vergences of parasitic fold structures). Since third order parasitic folding is present some vergences can face towards an antiform of a second order parasitic fold.

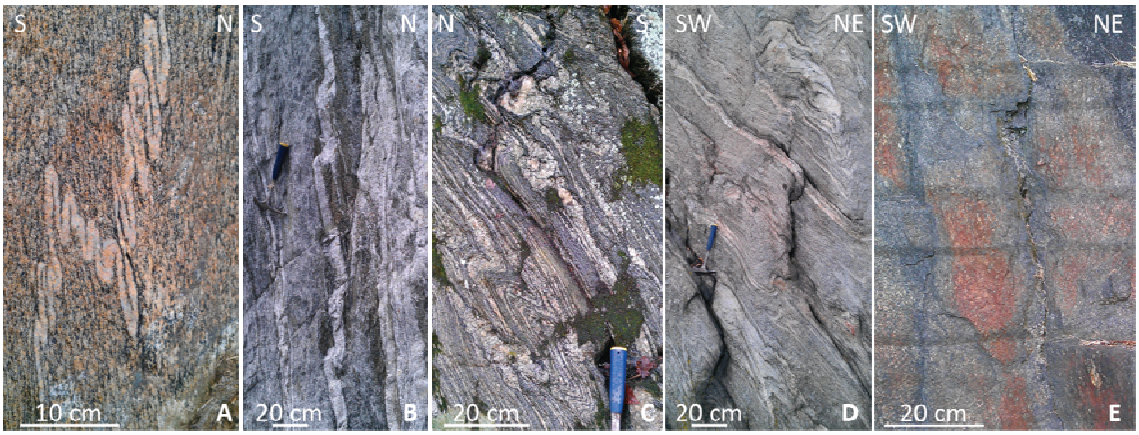

Figure 19 Parasitic folds
Origin: A and B outcrop 405, C outcrop 340, D outcrop 246, E outcrop 7
A shows two different orders of parasitic folding on a migmatite that has an antiform to the north. Few meters further north on image **B** parasitic folds style changed to much longer fold limbs kinky appearance. **C** is showing the D2 related folds in the highly folded zones. **D** shows the wide kinky folding that is observed in gneiss in the steep zone and **E** shows the D5 kinks in biotite schist where they stand out prominently.

Fold measurements

The foliation classification (S_1, S_2, etc.) of many measurements from the same outcrop is ambiguous because values are very similar. Orientation values are close to the ones of the lineation. There are likewise east and west dipping flat fold axes with a steeper group in the east.

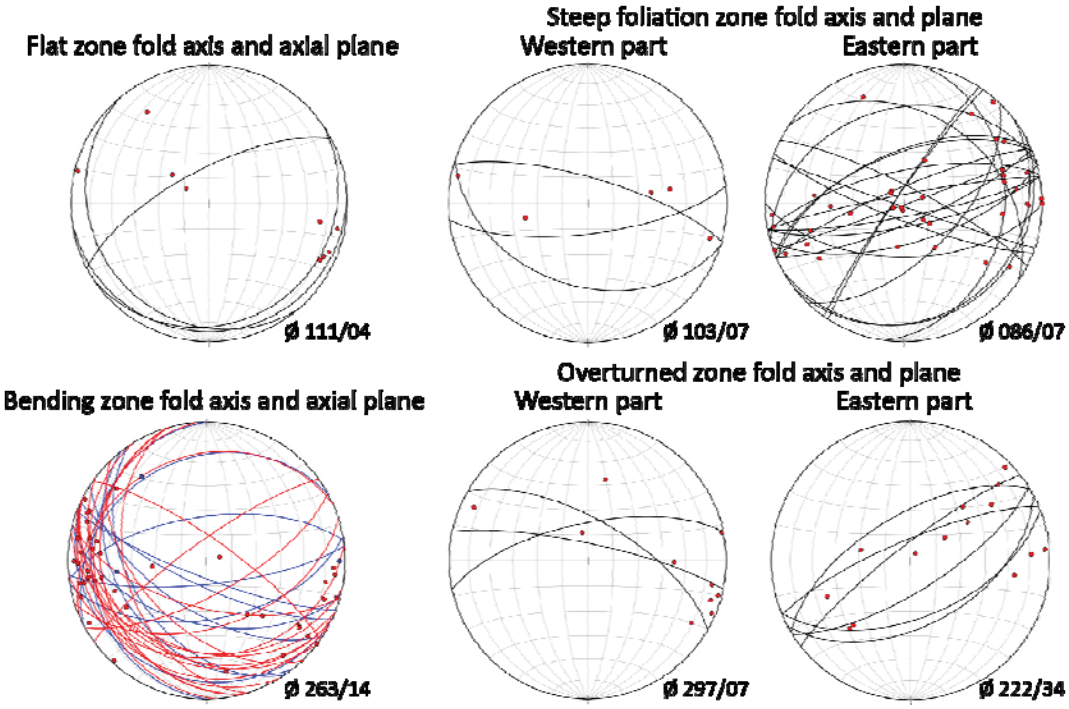

Figure 20 Stereoplots of fold axes and fold axial planes
The average values are maximum point density calculated with the Fisher distribution method.

Brittle structures

Faults

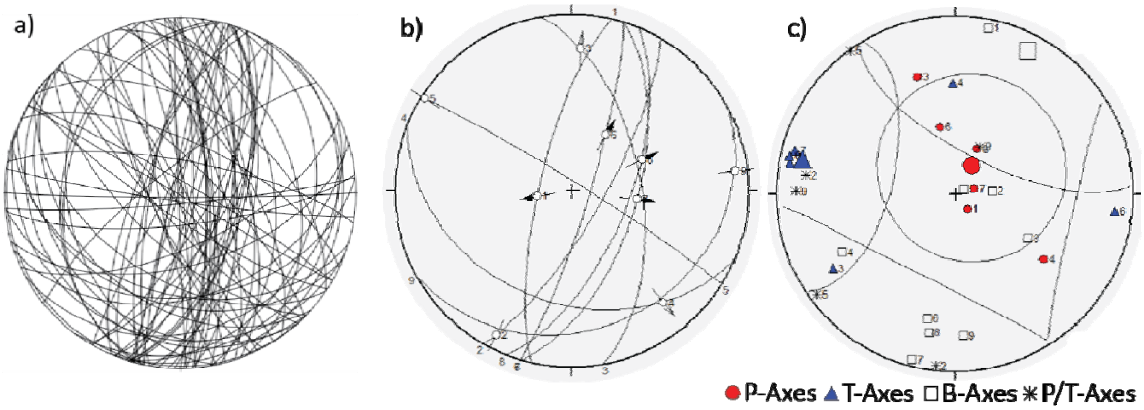

Figure 21 Stereoplots of analysed data from faults and slickenslides
Calculation made with Tectonics FP (REITER and ACS 1996).
a) Stereoplot of all 77 fault planes measured in the study area. The orientation of the planes fit to those used for the calculation.
b) Fault planes used for the calculation. Nine outcrops had a complete set of measurements that were used for the calculation.
c) Calculated Pressure axes (P-Axes) and tension axes (T-Axes) with Θ = 36°. Mean vector for pressure is 032/75 and for tension 283/13.

The brittle structures are mainly fault planes with slicken sides that strike more or less north-south. For the calculation in Figure 21 only complete and reliable measurements were used. Even though the result of the calculation is a normal fault it fits to the movement of the Insubric Fault which has dextral displacement and the normal faulting on Simplon Pass. If the calculated orientation with its sinistral displacement is turned a bit anticlockwise the expected dextral movement can be reached. The reason for this offset is due to selection of the measurements. Faults can be selected in a manner that the result is a perfectly fitting dextral normal fault.

There are also NW SE striking faults that are often valley forming (BÄCHLIN et al. 1974). They represent Riedel faults accompanying the Insubric Fault. These faults were not directly observed during field campaigns. They are considered as interpreted from the landscape.

The brittle structures postdate all other structures. They are homogenous throughout the field area. We do not have an age of these structures. But the fact that chlorite is often associated with the faults leads to the conclusion that these faults were generated under greenschist facies.

Figure 22 Cluster of small faults
Amphibolite with a cluster of sinistral joint-like faults. This can be explained with a block rotation in a big scale dextral shear zone such as the Insubric Fault. Amphibolite was brittle due to its mafic mineral content earlier than the surrounding more felsic gneisses.
Image was made on outcrop 142 at Alpe Cusale.

Fault gouge

Above Gorduno (outcrop 312) a several tens of meters wide fault gouge was observed. In this zone completely weathered reddish minerals can be easily scratched away by the hammer. Observation of this wide zone could not be measured but is assumed to be E-W striking and vertical. Another small thrust fault gouge that dips with ca. 35° to the south was observed (see Figure 23).

Figure 23 Fault gouge
The small structure at outcrop 405 has a top to the north movement. Here the fault contains still quartz up to millimetre size. The gouge material itself has no more cohesion. Due to the bending of the foliation it is assumed that the gouge was a shear zone prior to its alteration to a brittle gouge.

3D Models

The models intended to fit structures on the nappe scale. This aim was fulfilled in both models. The nappes are reflected in the model. The pink volume in the models represents the Southern Alps and deeper nappes that are not meaningful. They are modeled with some points south of the Piano di Magadino to enhance calculation below the Piano di Magadino. It is not known whether the Insubric Fault cut off the structures below the Piano di Magadino along the foliation or oblique to them. And even if it was cut obliquely the shearing would have made this angle almost invisible. The model includes no cutting of structures or a fault there.

The models were also calculated and analysed above the surface as e.g. shown in Figure 27 for Cima Lunga. The observed isoclinal folding style could not be modelled. Quaternary fill is not shown in the following figures. The bend into the Maggia Cross Fold is not visible because the modelled extend to the west is too small.

Model A (after STECK et al. 2013)

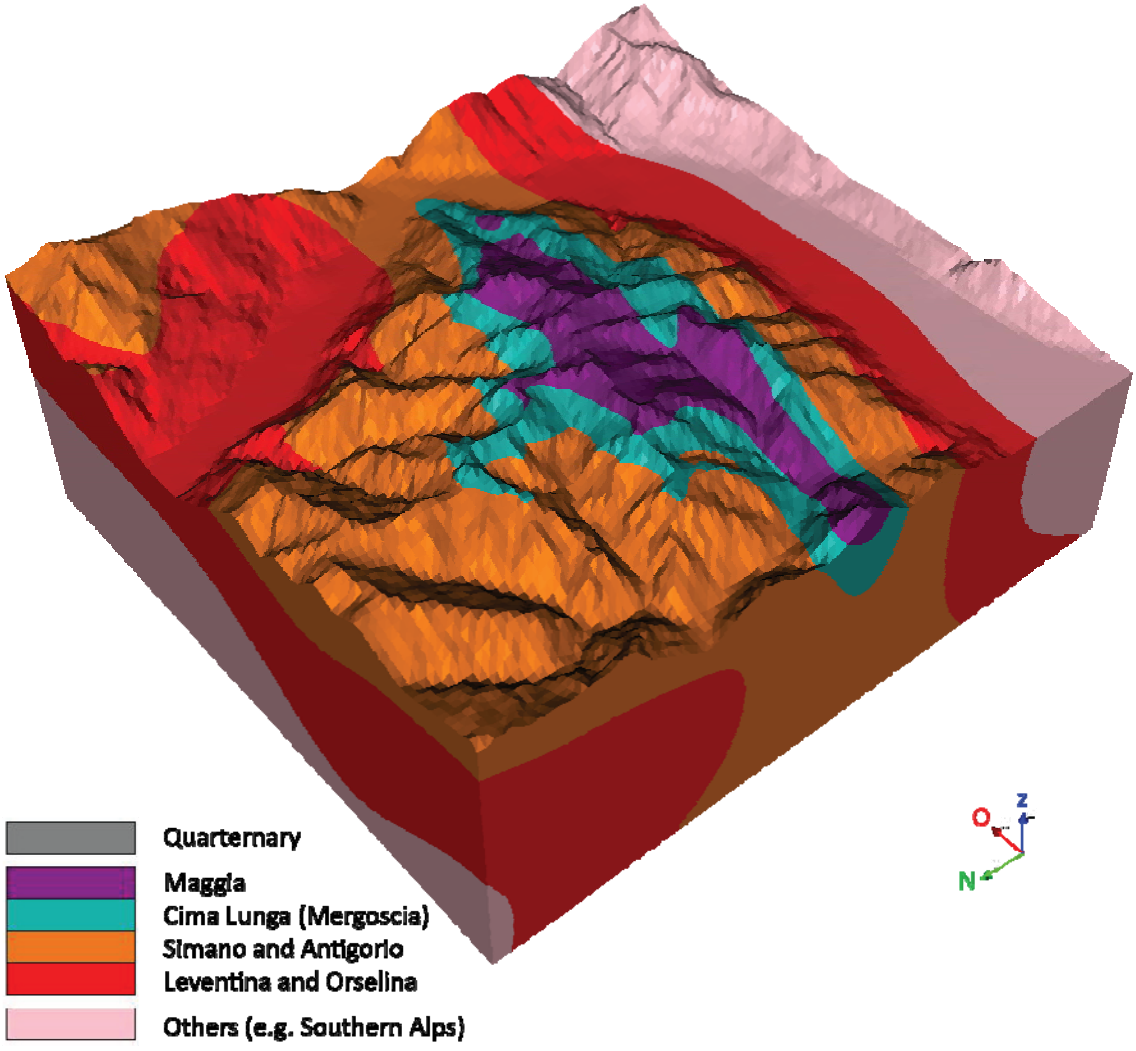

Figure 24 3D view from NW onto model A
Modelled input parameters are all on the surface

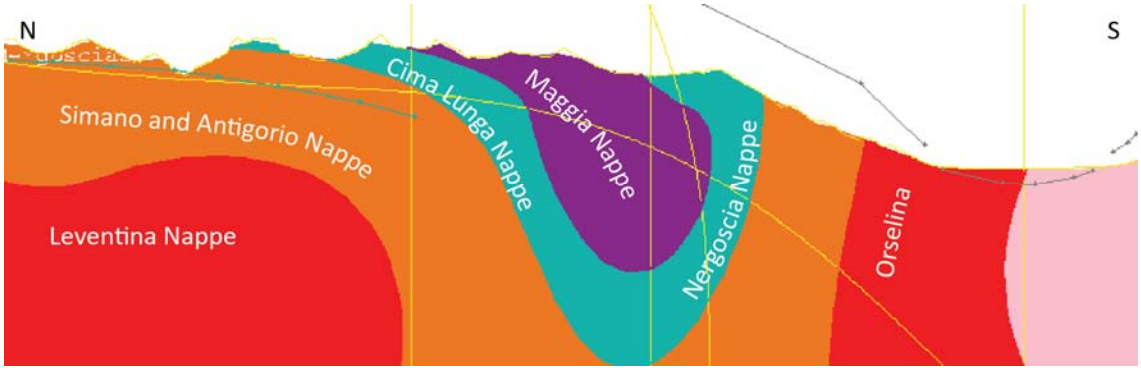

Figure 25 North-south section of model A
The yellow lines represent sections. The dots connected with lines represent inputted data.

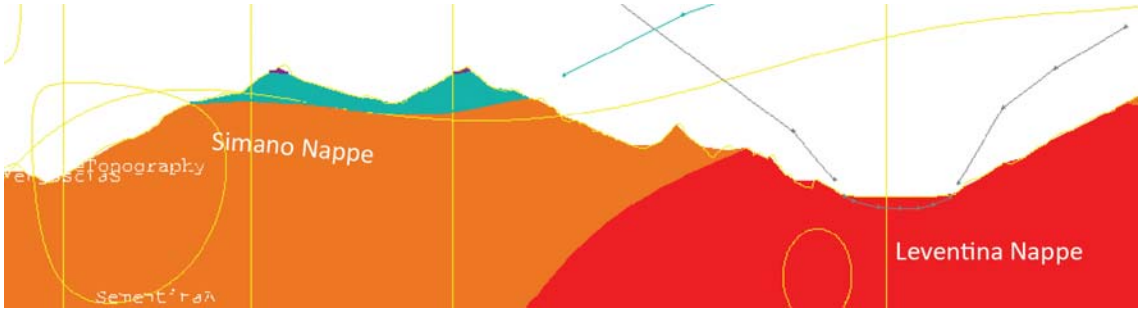

Figure 26 West-east section of model B

The model shows an ambos or mushroom shaped structure of the border between Leventina and Simano Nappe. It is not clear why this shape is modelled by GeoModeller it bases not on input data. The Sementina Fold structure is present but not where it should be. The fold crops out in Valle della Porta. The fold style is not isoclinal which caused a strange upper fold limb for the Maggia Nappe (see Figure 25).

Model B (after MAXELON and MANCKTELOW 2005)

The separation of the Cima Lunga Nappe on the surface and the correlation with Adula Nappe is modelled. Since the foliation data is the main source for the model the flat and the steep zones are represented quite well. Also the bend from SSW to SSE of the Southern Steep Belt between Valle di Verzasca and Bellinzona is modelled.

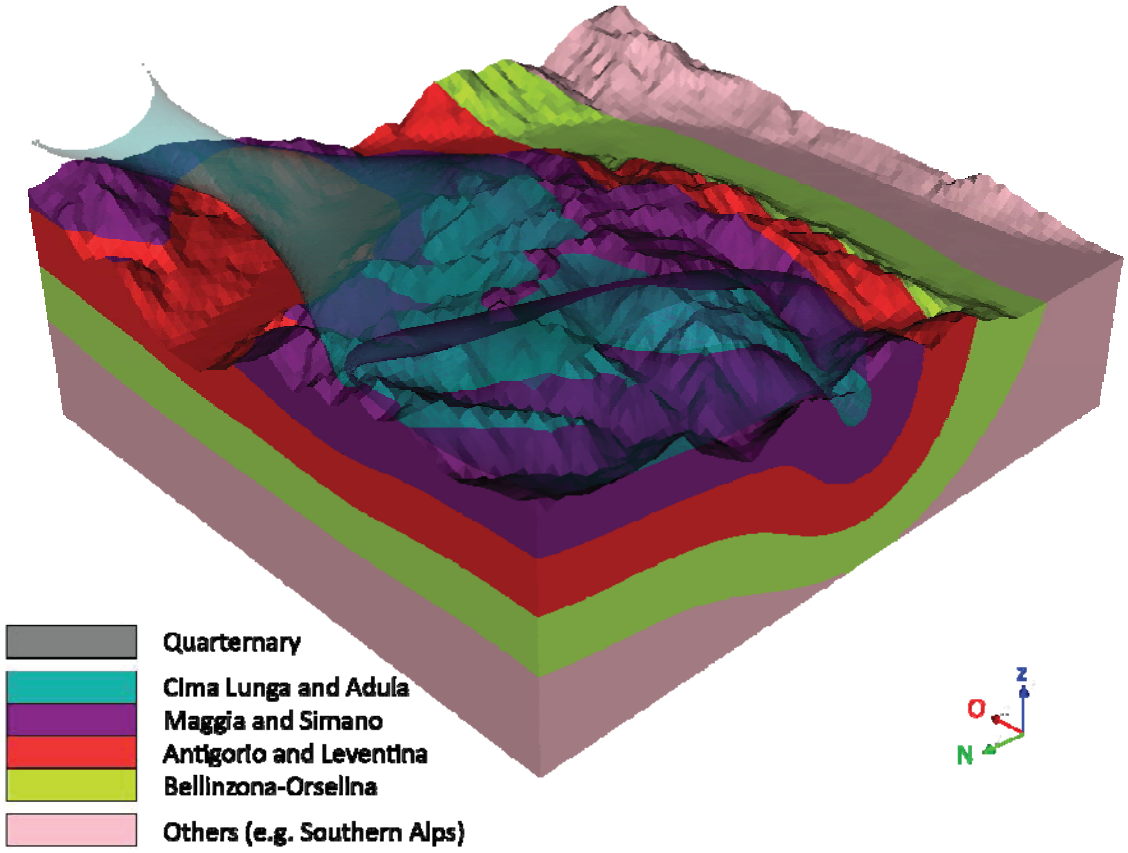

Figure 27 3D view from NW onto model B
Cima Lunga Nappe is shown with a blue transparent surface. The connection of Cima Lunga to the east created a tube above the surface. The parts below the red Leventina and Antigorio Nappes are not meaningful because they are not constrained by any input data.

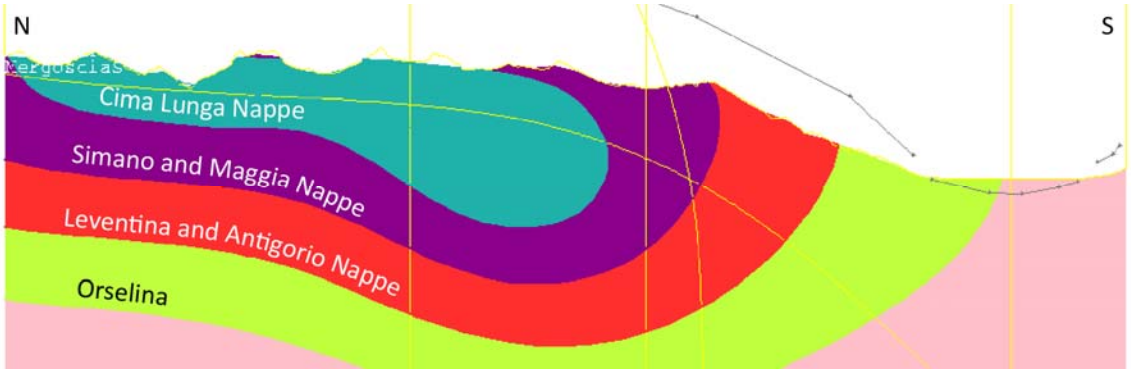

Figure 28 North-south section of model B
The section shows that the fold style is wrong. The isoclinal style cannot be modelled. Shown in yellow are two classical sections (straight lines) and two fold axial plane sections: The flat one is the Mergoscia Fold and the steeper one is the fold structure in the Valle di Sementina that was supposed to be modelled. The lines connecting dots are inputted contacts to model Quaternary sediment infill.

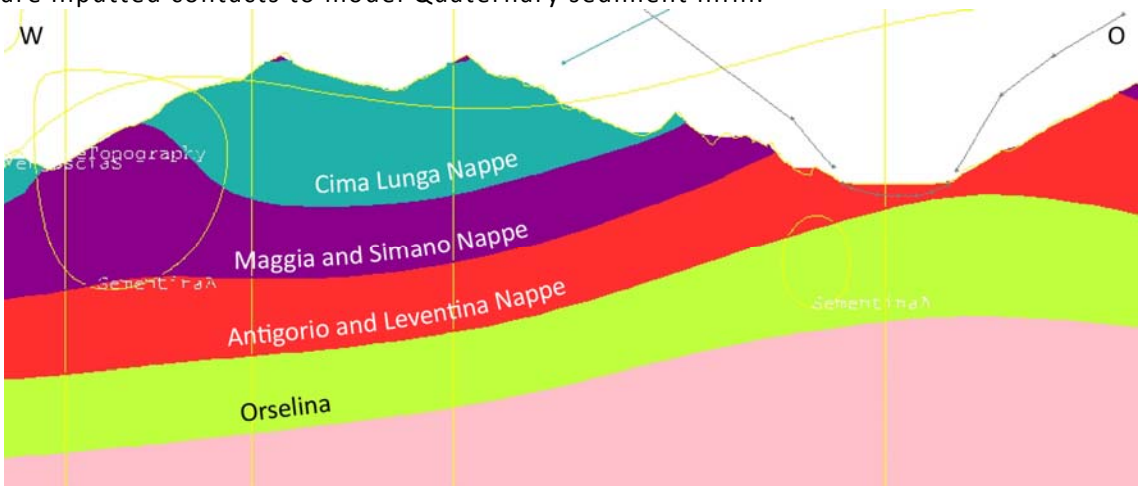

Figure 29 West-east section of model B
In the western part of the profile the model tries to follow the input contact data in Vogorno by lifting the contact higher than in areas where no close contact data is input. The section is very close to the modelled fold axial plane of the Sementina Fold that caused this odd egg shaped cuts in this section.

Interpretation and Discussion

Field data

The majority of the observed parasitic fold vergences in the Steep Belt suggest a closing fold structure to the south that was later overprinted by the bending of the Steep Belt. The antiform to the north can be caused by parasitic folds of third order on second order parasitic fold limbs. The early foliation of D1 and D2 was overprinted by the foliation of the subsequent deformation. Petrology on the other hand preserved the structures. On profile 3 in Figure 30 a fold is visible that has no more foliation remaining from the deformation. The fold is only recorded in petrological observations. The unusual geometry is illustrated in Figure 33. The reason for this structure may be a pre-existing fold.

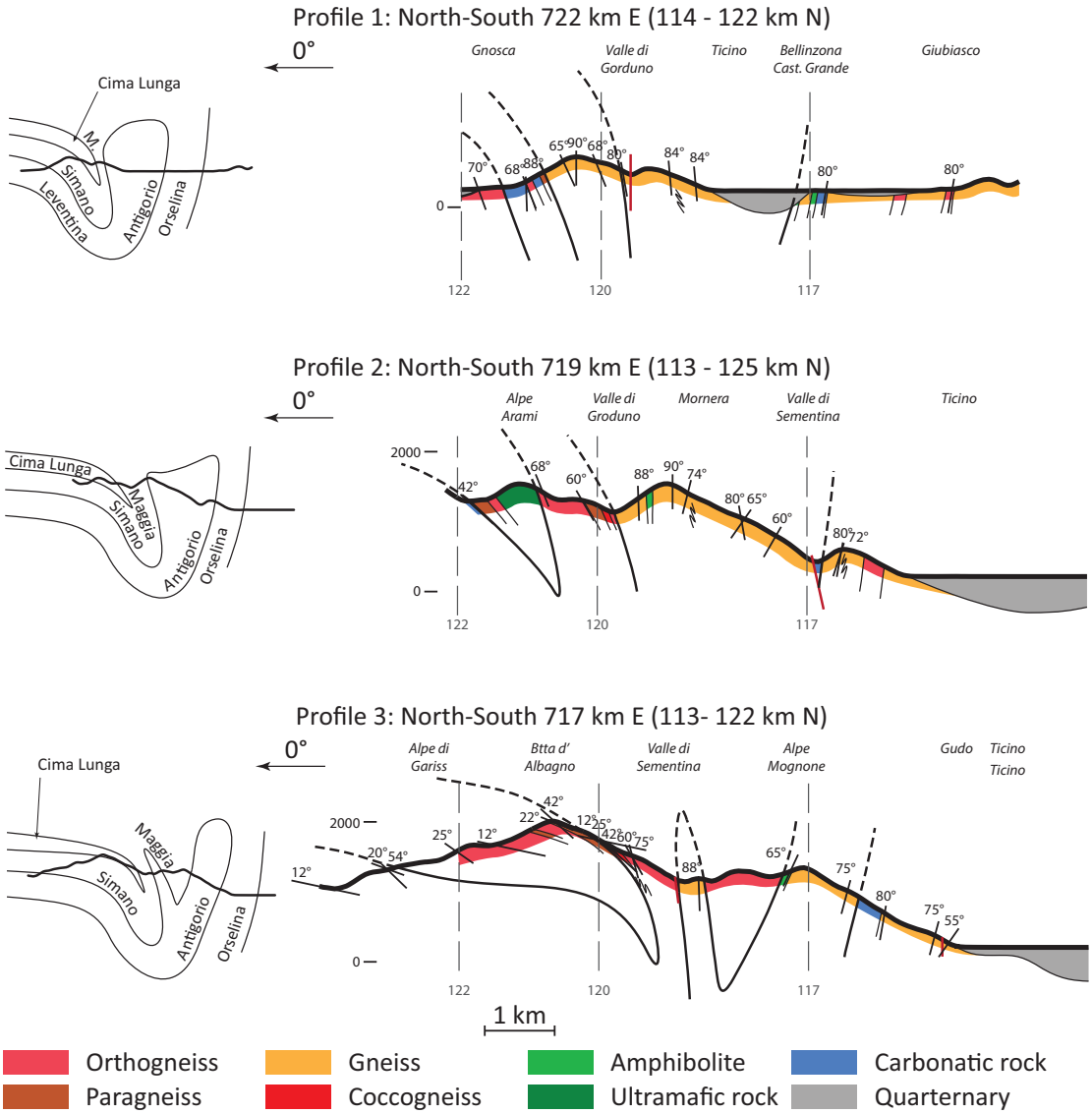

Figure 30 North south profiles 1 – 3
The corresponding tectonic sketch of the nappe situation is on the left. The nappe boundary interpretation is based on a manual extrapolation of the foliation data. The intersection with the surface is given by the petrological border of the nappe.

No parasitic folding is shown in Figure 30 and Figure 31 besides the main structure of profile 3 that indicates an antiform to the south on the larger scale. This is a simplification of the real situation. The boundaries of the nappes are strongly affected by parasitic isoclinal folding which makes it hard to define a nappe boundary.

On profile 5 and 6 in Figure 31 the bending gets tighter and the zone with vertical foliation gets wider. In the hinge of the Mergoscia fold the Cima Lunga Nappe is either complicatedly folded or imbricated. Profile 6 shows a section where the Maggia Cross Fold bends into the Steep Belt. Imbrication may be due to its position there.

The Antigorio Fold antiform disappears towards the east. Reason for this is given by the lineation at the Castelgrande in Bellinzona where the intersection lineation dips to the east (045/38). By crossing the Ticino River the nappe dives below the surface and is not observed anymore.

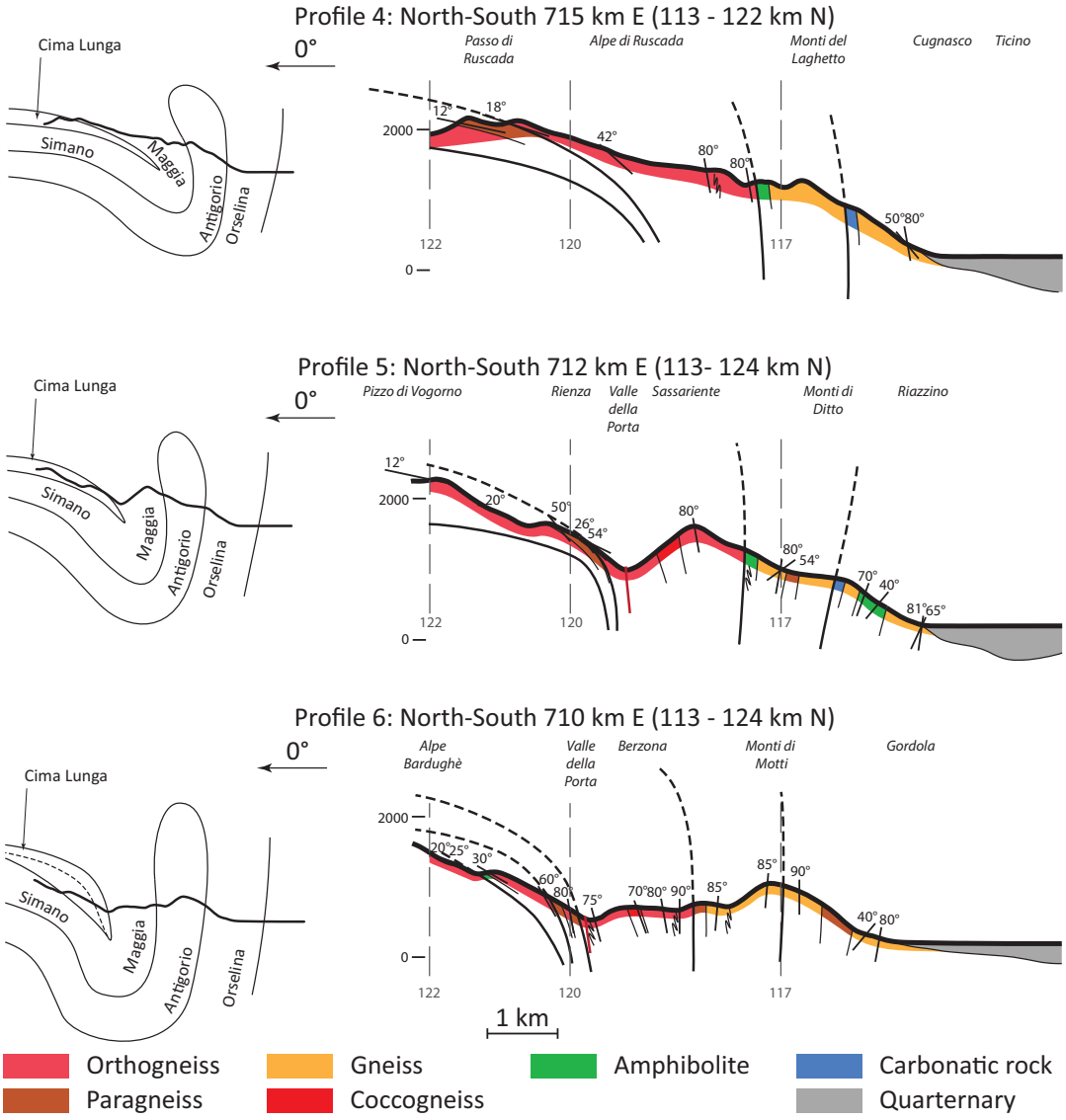

Figure 31 North south profiles 4 – 6
The corresponding tectonic sketch of the nappe situation is on the left.

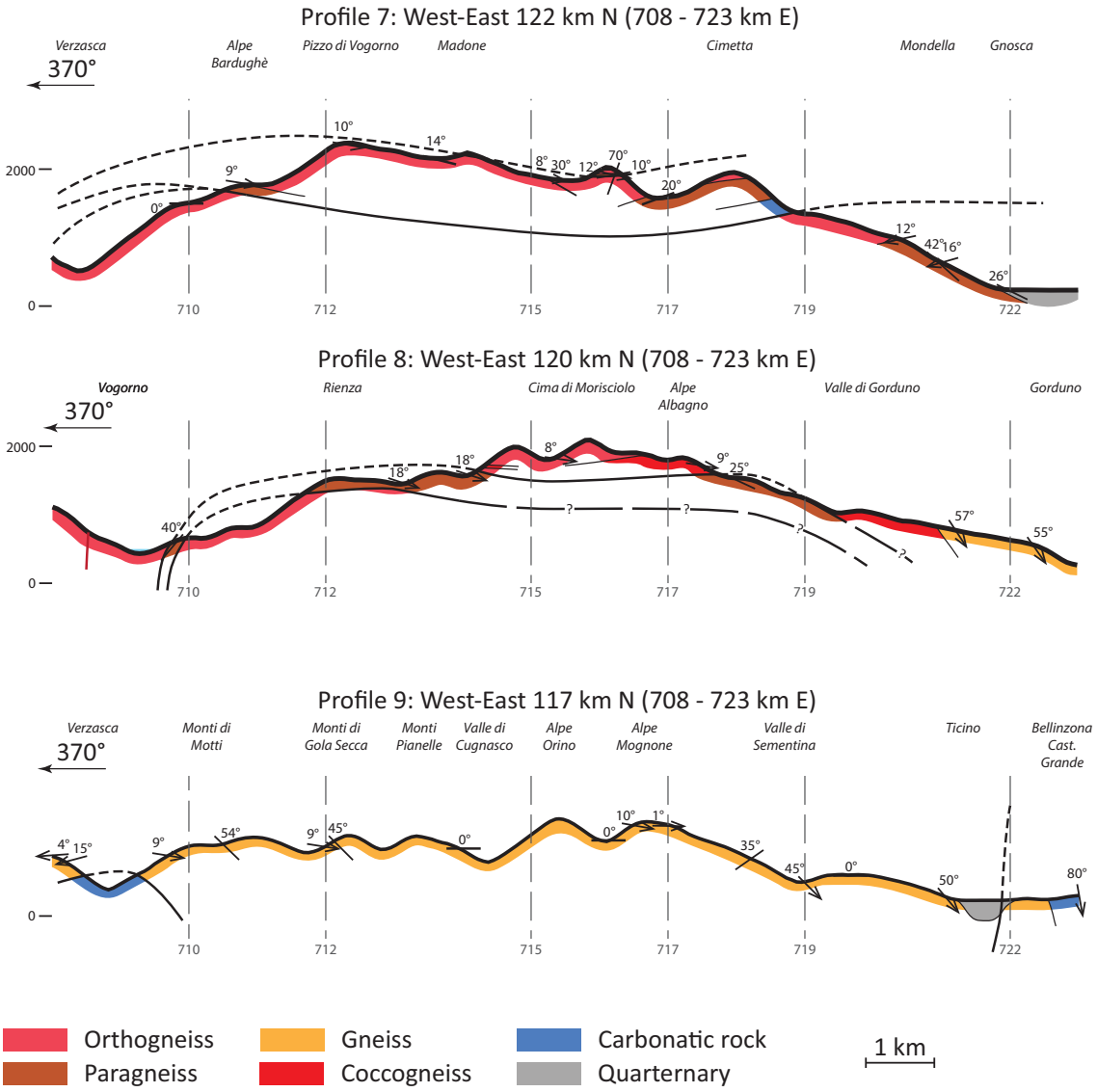

Figure 32 West east profiles 7 – 9
Profile 7 shows a synform to the north of Madone.

Folding structure in Valle di Sementina

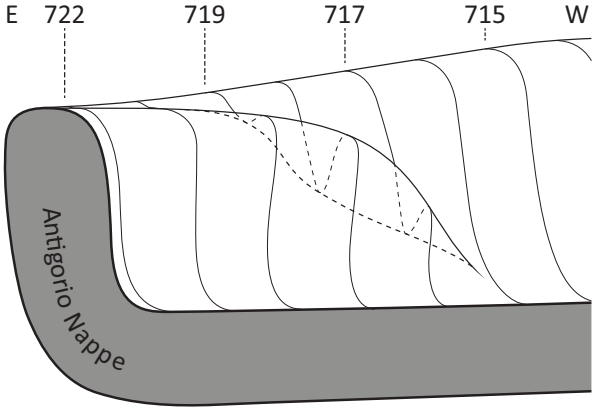

Figure 33 Sementina Fold
Schematic view to the south. The fold rises up from the bottom to the top of the main fold. This unusual M-style parasitic fold where the northern limb raises up on the side has no more foliation and only hints from steeper dipping lineations. The structure is only evident on the geological map.
The number refers to the easting of the profiles of Figure 30 and Figure 31.

The key to understanding the geology in the Lepontine dome north of the Insubric Fault lies in the explanation of the Maggia Cross Folding zone. The first deformation phases are quite clear; the steep zones are already associated with open questions but the formation of the north-south fold striking axes - with the Maggia Cross Fault as its prominent representative - is still controversial in terms of timing and genesis. The question on what caused the special deformation pattern of the Maggia Cross Fold has to be answered to get a coherent model.

To discriminate the folding phases the observations of the fold style plays an important role. The observations until now agree with observations done by HUBER et al. (1980) who related these types with the fold phases. The three observed foliations require at least three deformation phases and because the folds axis orientations differ by a large angle a change in the big scale compression regime was needed.

The antiform to the south observations can be explained by the big scale folding model of MAXELON and MANCKTELOW (2005) or by interference of folding and shearing model of PLEUGER et al. (2008).

Migmatisation is present in the whole study area. The amount of migmatites in the south east is only slightly increased compared with the northern areas. Migmatites are found mainly in orthogneiss. The grade of migmatisation is not helpful for a detailed separation of nappes.

Paleogeography

For the reconstruction of the paleogeography the study of Deutsch (1979) about rodingites in mafic lenses in the Adula Nappe (Cima Sgiu) has to be considered. Rodingites are mafic rocks (basaltic composition) that developed through a metasomatic reaction with calcium from oceanic waters (LI et al. 2004). Metamorphosed blackwalls have break down reactions to olivine, enstatite and spinel (Frost 1975). Outcrops in the Adula Nappe that have rodingites or associated blackwalls are therefore interpreted as former oceanic crust (Deutsch 1979).

Ocean basalt interactions that caused metarodingites are a clear sign for an active spreading centre. According to the tectonic position of the Maggia Nappe the rodingites are from the Valais Trough or the Piemont-Ligurian Ocean. With the nappe model of STECK et al. (2013) the mafic lenses in Cima Lunga Nappe can be explained by the slow and discontinued spreading of the Valais Ocean. With the model of MAXELON and MANCKTELOW (2005) Cima Lunga is assigned to the Piemont-Ligurian Ocean.

3D Model

The handicap that only surface data was entered into the model could not be improved by introducing virtual contact data and fold axial traces in cross sections. As it is visible in Figure 28 isoclinal folding cannot be modelled correctly. All folds remained open folds although they are all isoclinal besides the steepening.

In Valle di Sementina there is a fold structure that cannot be resolved with GeoModeller. The problem is that the later foliation overprinted the structure. This case is conflict with the hypothesis for the model that relies mainly on foliation data. The folding structure is only seen on the geological map due to its petrology but not on foliation. The input of lineation data or fold axis cannot correct the model. In model A selection of normal overturned foliation allowed modeling of a fold like structure whereas in model B nothing like a fold could be generated.

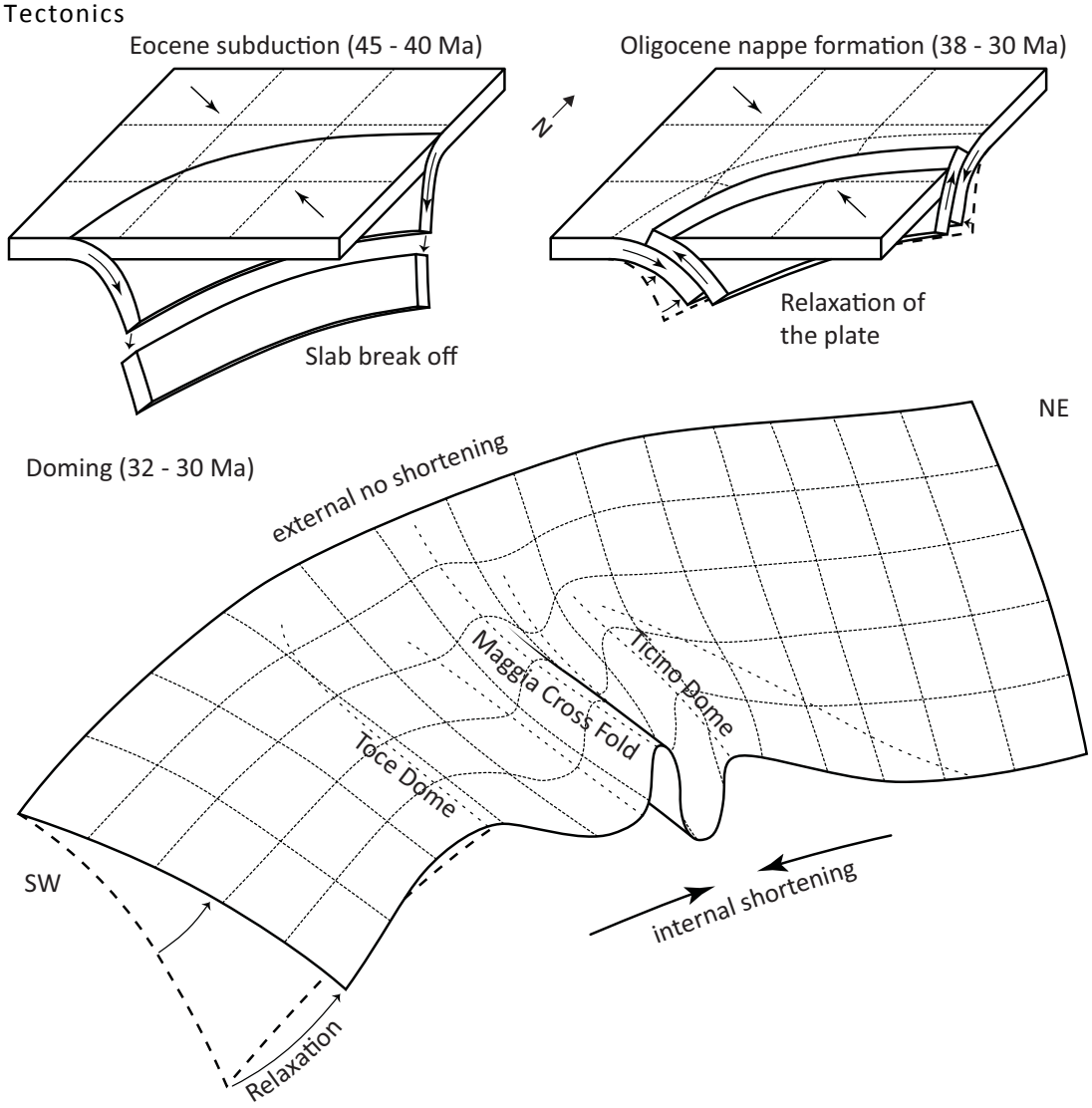

Figure 34 Schematic sketch of the evolution of the Maggia Cross Fold and the domes The arc shaped Alpine front lead to strain when the European plate was subducted. Nappe formation and cross folds can coevally form because the NW – SE stress is tectonically caused and the SW – NE shortening is related to the relaxation of the plate after the slab break off.

The interpretation of how the Maggia Cross Fold developed is still unclear. The deformation phases are all overlapping starting with nappe emplacement 38 Ma ago or even earlier in the south until formation of the Southern Steep Belt at 25 Ma (BERGER et al. 2005). The slab break off at 45 to 40 Ma removed load and started a process of plate relaxation and uplift (BLANCKENBURG and DAVIES 1995). The plate that could earlier be subducted oblique to the Alpine front - orthogonal to the plate movement of the intender – relaxes later without the possibility of lateral escape and stays confined on its sides de due the arc shaped form of the Alps (see Figure 2). This leads to a shortening of the internal part of the subducted plate contemporaneously with its relaxation. This space issue gets more accentuated the more this process proceeds. Meaning that first the nappe formation dominates the process, then the back folding due to uplift starts before the cross folding dominates the deformation of the Penninic Nappes. The tightening of the folds towards the Insubric Fault is

also explainable by the relaxation cross folding. There is less space in the internal parts and this causes narrower folds. Towards the end of the relaxation the Southern Steep Belt developed simultaneously with the proto Insubric Fault shear zone. When the fault became brittle it cut the Steep Belt folding, partly in an oblique manner.

The extent of the Lepontine can be connected to the Bouger anomalies in the Ivrea body due to the lighter rock composition (CASSINIS 2006). The two sub domes are right adjacent to the anomaly. Toce subdome is right behind and Ticino subdome right east of it. To the east there is no arc present that could cause a space problem when the plate relaxes.

Conclusion

1. The tectonic stratigraphic pile of the nappes west and east of the Lepontine Dome can be correlated differently. The consistent parasitic fold vergences (antiform to the south) support the correlation of Maggia and Simano Nappes.
2. After the fist nappe emplacement east-west shortening deformation caused the tight to isoclinal Maggia Cross Fold. This structure was either simultaneous with or prior to the formation of the Southern Steep Belt.
3. The formation of the Maggia Cross Fold may be related to slab break-off and the subsequent back folding. The arc shaped form of the Alps caused internal shortening when the remaining slab relaxed and caused uplift.
4. GeoModeller is not designed to model regions where the stratigraphy is unknown. Since GeoModeller uses potential field theory to calculate it needs a defined succession for all modelled formations and information on the polarity at every point that is entered into the model.

Open questions to be resolved

The tectonic model is an idea to explain field observations. A kinematic model for the tectonic model should be done to check whether the relaxation effect can cause cross folding.

The correlation of nappes leads to a new question: Do both the Maggia and Simano Nappes belong to the Briançonnais and therefore to the Middle Penninic domain? Or is only a small upper proportion of the Simano Nappe Middle Penninic? Hints towards this are given in the detailed study of the northern parts of the Adula Nappe by (GALSTER et al. (2010)).

Acknowledgements

The Geological Institute of ETH Zürich is thanked for the funding of the thesis. Manuele Lazzarotto writes a complementary thesis to this thesis; we share common data such as measurements and had fertile discussions. Giorgio Valenti from the *Sezione forestale Repubblica e Cantone Ticino* is thanked for providing cadastre maps. Barbara Kuhn is thanked for her useful tips in the field and for the description of the thin sections. I also thank the Lazzarotto family in Bellinzona for the hospitality during field campaigns. The *Patriziato di Gudo* and *SEV (Società Escursionistica Verzaschese)* are thanked for the special conditions for the hut usage.

References

ALLMENDINGER Richard W, CARDOZO Nestor and FISHER Donald M, 2012. Structural Geology Algorithms: Vectors and Tensors. Cambridge University Press.

BÄCHLIN R, BIANCONI F, CODONI A, DAL VESCO E, KNOBLAUCH P, KÜNDIG E, REINHARD M, SPAENHAUER F, SPICHER A and TROMMSDORFF V, 1974. Geologischer Atlas der Schweiz, 1: 25 000, Blatt 1313 Bellinzona. Schweizerische Geologische Kommission, Bern, Switzerland. Gaggio-Basal (cantone Ticino). Schweiz. Mineral. Petrogr. Mitt, 33: 173-480.

BERGER Alfons, MERCOLLI Ivan and ENGI Martin, 2005. The central Lepontine Alps: Notes accompanying the tectonic and petrographic map sheet Sopra Ceneri (1: 100,000). Schweizerische Mineralogische und Petrographische Mitteilungen, 85: 109-146.

BLANCKENBURG Friedhelm and DAVIES J Huw, 1995. Slab breakoff: a model for syncollisional magmatism and tectonics in the Alps. Tectonics, 14(1): 120-131.

BURRI Thomas, 2005. From High-pressure to Migmatisation: On Orogenic Evolution of the Southern Lepontine (Central Alps of Switzerland/Italy). Inauguraldissertation Thesis, Bern, Universitätsbibliothek Bern, 159 pp.

BURRI Thomas, BERGER Alfons and ENGI Martin, 2005. Tertiary migmatites in the Central Alps: Regionaldistribution, field relations, conditions of formation and tectonic implications. Schweizerische Mineralogische und Petrographische Mitteilungen, 83: 215-235.

BUSSIEN Denise, BUSSY François, MAGNA Tomas and MASSON Henri, 2011. Timing of Palaeozoic magmatism in the Maggia and Sambuco nappes and paleogeographic implications (Central Lepontine Alps). Swiss Journal of Geosciences, 104(1): 1-29.

CASSINIS Roberto, 2006. Reviewing pre-TRANSALP DSS models. Tectonophysics, 414(1): 79-86.

CHILÈS Jean-Paul, AUG Christophe, GUILLEN Antonio and LEES Terry, 2004. Modelling the geometry of geological units and its uncertainty in 3D from structural data: the potential-field method, Proceedings of International Symposium on Orebody Modelling and Strategic Mine Planning, Perth, Australia, pp. 313-320.

DEUTSCH A, 1979. Serpentinite und Rodingite der Cima Sgiu (NW Aduladecke, Ticino). Schweiz Mineral Petrogr Mitt, 59: 319-347.

ENGI M, BOUSQUET R and BERGER A, 2004. Metamorphic structure of the alps: Central alps. Explanatory notes to the map of metamorphic structures of the Alps. Mitteilungen der Österreichischen Mineralogischen Gesellschaft, 149: 157-173.

EPARD Jean-Luc and ESCHER Arthur, 1996. Transition from basement to cover: a geometric model. Journal of Structural Geology, 18(5): 533-548.

ESCHER Arthur and BEAUMONT Christopher, 1997. Formation, burial and exhumation of basement nappes at crustal scale: a geometric model based on the Western Swiss-Italian Alps. Journal of Structural Geology, 19(7): 955-974.

FROITZHEIM Nikolaus, PLEUGER Jan, ROLLER Sybille and NAGEL Thorsten, 2003. Exhumation of high-and ultrahigh-pressure metamorphic rocks by slab extraction. Geology, 31(10): 925-928.

FROST B Ronald, 1975. Contact metamorphism of serpentinite, chloritic blackwall and rodingite at Paddy-Go-Easy Pass, Central Cascades, Washington. Journal of Petrology, 16(1): 272-313.

GALLI Andrea, MANCKTELOW Neil, REUSSER Eric and CADDICK Mark, 2007. Structural geology and petrography of the Naret region (northern Valle Maggia, N. Ticino, Switzerland). Swiss Journal of Geosciences, 100(1): 53-70.

GALSTER Federico, EPARD Jean-Luc, MASSON Henri and CAVARGNA-SANI Mattia, 2010. The Soja and Luzzone-Terri nappes ; discovery of a Briaçonnais element below the front of the Adula nappe (NE Ticino, Central Alps) ; Discovery of fossils in the Adula nappe, new stratigraphic data and tectonic consequences (Central Alps). Bulletin de géologie Lausanne, 368.

GANSSER Augusto, 1968. The Insubric Line, a major geotectonic problem. Geologisches Institut der Eidg. Technischen Hochschule und der Universität Zürich.

GEBAUER Dieter, 1996. A PTt path for an (ultra?-) high-pressure ultramafic/mafic rock-association and its felsic country-rocks based on SHRIMP-dating of magmatic and metamorphic zircon

domains. Example: Alpe Arami (Central Swiss Alps). Geophysical Monograph Series, 95: 307-329.

GEBAUER Dieter, 1999. Alpine geochronology of the Central and Western Alps: new constraints for a complex geodynamic evolution. Schweizerische Mineralogische und Petrographische Mitteilungen, 79(1): 191-208.

GROHMANN CH and CAMPANHA GA, 2010. OpenStereo: open source, cross-platform software for structural geology analysis, AGU Fall Meeting abstracts, pp. 06.

GROND Reto, WAHL Felix and PFIFFNER Marcel, 1995. Polyphase Alpine deformation and metamorphism in the northern Cima lunga unit, Central Alps (Switzerland). Schweizerische Mineralogische und Petrographische Mitteilungen, 75(3): 371-386.

GRUJIC Djordje and MANCKTELOW Neil S, 1996. Structure of the northern Maggia and Lebendun nappes, central Alps, Switzerland. Eclogae Geologicae Helvetiae.

HUBER Martin, RAMSAY John and SIMPSON Carol, 1980. Deformation in the Maggia and Antigorio nappes, Lepontine Alps. Eclogae Geologicae Helvetiae, 73(2): 593-606.

LI Xu-Ping, RAHN Meinert and BUCHER Kurt, 2004. Metamorphic processes in rodingites of the Zermatt-Saas ophiolites. International Geology Review, 46(1): 28-51.

LIATI A, GEBAUER D and FANNING M, 2000. U-PbSHRIMP dating of zircon from the Novate granite (Bergell, Central Alps): evidence for Oligocene-Miocene magmatism, Jurassic/Cretaceous continental rifting and opening of the Valais trough. Schweizerische mineralogische und petrographische Mitteilungen, 80(3): 305-316.

MAXELON Michael and MANCKTELOW Neil S, 2005. Three-dimensional geometry and tectonostratigraphy of the Pennine zone, Central Alps, Switzerland and Northern Italy. Earth-Science Reviews, 71(3): 171-227.

MCINERNEY Philip, GUILLEN Antonio, COURRIOUX Gabriel, CALCAGNO Philippe and LEES Terry, 2005. Building 3D geological models directly from the data? A new approach applied to Broken Hill, Australia. Digital Mapping Techniques, 5: 119-130.

MERLE Oliver, COBBOLD PR and SCHMID S, 1989. Tertiary kinematics in the Lepontine dome. Geological Society of London Special Publications, 45: 113-134.

MERLE Olivier and LE GAL Philippe, 1988. Post-amphibolitic westward thrusting and fold vergence in the Ticino domain. Eclogae Geologicae Helvetiae, 81(1): 215-226.

MILNES Alan Geoffrey, 1974. Structure of the Pennine Zone (Central Alps): a new working hypothesis. Geological society of America bulletin, 85(11): 1727-1732.

NAGEL Thorsten, DE CAPITANI C, FREY M, FROITZHEIM N, STUNITZ H and SCHMID SM, 2002. Structural and metamorphic evolution during rapid exhumation in the Lepontine dome (southern Simano and Adula nappes, Central Alps, Switzerland). Eclogae Geologicae Helvetiae, 95(3): 301-321.

ORTNER Hugo, REITER Franz and ACS Peter, 2002. Easy handling of tectonic data: the programs TectonicVB for Mac and TectonicsFP for Windows™. Computers & Geosciences, 28(10): 1193-1200.

PFIFFNER Marcel, 1999. Genese der hochdruckmetamorphen ozeanischen Abfolge der Cima Lunga-Einheit (Zentralalpen).

PFIFFNER Othmar Adrian, 2009. Geologie der Alpen. Haupt.

PLEUGER Jan, NAGEL Thorsten J, WALTER Jens M, JANSEN Ekkehard and FROITZHEIM Nikolaus, 2008. On the role and importance of orogen-parallel and-perpendicular extension, transcurrent shearing, and backthrusting in the Monte Rosa nappe and the Southern Steep Belt of the Alps (Penninic zone, Switzerland and Italy). Geological Society, London, Special Publications, 298(1): 251-280.

PREISWERK Heinrich, 1921. Die zwei Deckenkulminationen Tosa-Tessin und die Tessiner Querfalte. Buchdr. Emil Birkhäuser.

PREISWERK Heinrich, 1931. Der Quarzdiorit des Coccomassives (zentrale Tessineralpen) und seine Beziehungen zum Verzascagneis. Schweizerische Mineralogische und Petrographische Mitteilungen, 11: 28.

PREISWERK Heinrich, JEANNET Alphonse and KRIGE Leo J, 1918. Geologische Karte des oberen Tessin und Maggia-Gebietes. Schweizerische Geologische Kommission.

REITER F. and ACS P., 1996. TectonicsFP: Software for structural geology. Innsbruck Univ., Innsbruck, Austria.

ROMER RL, SCHÄRER U and STECK Albrecht, 1996. Alpine and pre-Alpine magmatism in the root-zone of the western Central Alps. Contributions to Mineralogy and Petrology, 123(2): 138-158.

RUBATTO Daniela, HERMANN Jörg, BERGER Alfons and ENGI Martin, 2009. Protracted fluid-induced melting during Barrovian metamorphism in the Central Alps. Contributions to Mineralogy and Petrology, 158(6): 703-722.

RÜTTI Roger, MAXELON Michael and MANCKTELOW Neil S, 2005. Structure and kinematics of the northern Simano nappe, Central Alps, Switzerland. Eclogae Geologicae Helvetiae, 98(1): 63-81.

SCHMID SM, ZINGG A t and HANDY M, 1987. The kinematics of movements along the Insubric Line and the emplacement of the Ivrea Zone. Tectonophysics, 135(1): 47-66.

SCHMID Stefan M, FÜGENSCHUH Bernhard, KISSLING Eduard and SCHUSTER Ralf, 2004. Tectonic map and overall architecture of the Alpine orogen. Eclogae Geologicae Helvetiae, 97(1): 93-117.

SIMPSON C and WINTSCH RP, 1989. Evidence for deformation-induced K-feldspar replacement by myrmekite. Journal of Metamorphic Geology, 7(2): 261-275.

SPICHER August, SPICHER August, GÉOLOGUE Minéralogiste, SPICHER August, GEOLOGIST Mineralogist and CARTOGRAPHER Switzerland, 1980. Tektonische Karte der Schweiz. Bundesamt für Landestopographie.

STECK Albrecht, 1998. The Maggia cross-fold: An enigmatic structure of the Lower Penninic nappes of the Lepontine Alps. Eclogae Geologicae Helvetiae, 91(3): 333-343.

STECK Albrecht, 2008. Tectonics of the Simplon massif and Lepontine gneiss dome: deformation structures due to collision between the underthrusting European plate and the Adriatic indenter. Swiss Journal of Geosciences, 101(2): 515-546.

STECK Albrecht, DELLA TORRE Franco, KELLER Franz, PFEIFER Hans-Rudolf, HUNZIKER Johannes and MASSON Henri, 2013. Tectonics of the Lepontine Alps: ductile thrusting and folding in the deepest tectonic levels of the Central Alps. Swiss Journal of Geosciences: 1-24.

STOCK JM and HODGES KV, 1989. Pre-Pliocene Extension around the Gulf of California and the transfer of Baja California to the Pacific Plate. Tectonics, 8(1): 99-115.

SWISSTOPO Bundesamt für Landestopografie, 2001. DHM 25.

SWISSTOPO Bundesamt für Landestopografie, 2005. Geologische Karte der Schweiz, 1: 500,000. Wabern, Switzerland.

SWISSTOPO Bundesamt für Landestopografie, 2008a. 1293 OSOGNA 1:25000.

SWISSTOPO Bundesamt für Landestopografie, 2008b. 1313 BELLINZONA 1:25000.

WENK Eduard, 1953. Prinzipielles zur geologisch-tektonischen Gliederung des Penninikums im zentralen Tessin. Eclogae Geologicae Helveticae, 46: 9-21.

WENK Eduard, 1955. Eine Strukturkarte der Tessineralpen.

WENK Eduard, 1982. Tonalite und Granodiorite des Cocco-Zuges. Schweizerische mineralogische und petrographische Mitteilungen, 62(1): 8.

Appendix

Table of all outcrops

Table contains coordinates, elevation and all information for an outcrop.

Table of all measurements

Table contains the list

Lithology and migmatisation

Fold-out map 1:40’000 with format A3.

Vergences of parasitic fold structures

Fold-out map 1:40’000 with format A3.

Field observations

Detachable map 1:20’000 with format 76x56.

Foliation

Detachable map 1:20’000 with format 76x56.

Lineations

Detachable map 1:20’000 with format 76x56.

Fold structures

Detachable map 1:20’000 with format 76x56.

Faults

Detachable map 1:20’000 with format 76x56.

Declaration of originality

Table of all outcrops

Coordinate system (E and N): Swiss national grid CH1903

Nr	E	N	Elevation	Lithology	Sample	Image	Anticline	Migmatites	Shearing
1	720342	122215	938	PG					
2	720262	122289	920			IMAG0230			
3	720124	122570	880						
4	720536	122254	830		1				
5	720647	122180	820						
6	721006	121806	680	PG	2		S		
7	721161	122467	430	PG			S		
8	721114	122544	400						
9	722517	118846	255	PG		Yes (Neil)		Yes	Augen. S up
10	720364	116569	250	PG	3				Augen, S up
11	717889	119267	1650	OG			S		
12	717816	119333	1680						
13	717566	119510	1770	CG				Yes	
14	717354	119722	1820	OG					
15	717377	119829	1880	PG	4				
16	717325	119906	1900	PG					
17	717430	121047	2185	Am	5				
18	716900	120486	1980	Am					
19	716840	120459	1990				S		
20	716818	120445	1995		2a		S		Quartz, thrust fault to N
21	716750	120469	2020						
22	716725	120537	2050						Clast, thrust fault to N
23	716718	120572	2060						
24	716428	120637	2200						
25	716609	120619		CG			N		
26	716306	120568	2225						
27	715974	120744	2240				S		
28	715854	120887	2280	CG		Panorama			
29	715791	120962	2280	CG					
30	715679	121283	2390	PG	7		S		
31	717038	120260	1867	PG					
32	716882	120239	1910	CG					
33	716780	120161	1920	CG					
34	716769	120127	1920			Yes			
35	716690	120079	1930						
36	716591	120024	1920	PG					
37	716592	119993	1915	OG					
38	717097	120135	1870	OG	10		S	Yes	Shearband, thrust to NE
39	716924	120146	1850	OG					
40	716858	119833	1740						
41	716685	119857	1770	OG					
42	716660	119617	1680	OG			S		
43	716714	119538	1570	OG				Yes	
44	716791	119541	1550	OG					
45	716842	119567	1577	PG	8				
46	716882	119632	1555	OG			S		
47	717058	119479	1551	OG					
48	717102	119438	1528	OG					
49	717245	119342	1489	OG			S	Yes	
50	717311	119283	1472	OG			N		
51	717350	119213	1425	OG			S	Yes	
52	717441	119152	1390	OG			S		
53	717483	119133	1400	OG			S		
54	717645	119078	1425	OG					
55	717814	119022	1444	OG				Yes	
56	717859	119000	1447	CG					
57	718017	118825	1457						
58	718191	118666	1465	CG					
59	718949	118704	1409						
60	711606	117391	1028	CG					
61	711617	117336	1028						
62	711599	117298	1026				S		
63	722495	118797	250	PG		Yes			
64	722465	118727	250	PG				Yes	
65	712313	116731	1095	OG			S	Yes	South down
66	712541	117027	1128	OG		4998, 5000	S	Yes	
67	712512	117079	1134	OG			S		
68	712921	117591	1202	CG					
69	713230	117507	1240	CG					
70	713290	117422	1245	OG					
71	713571	117774	1500	OG					
72	714011	118676	1685	Am			N		

73	714419	119202	1805	CG					
74	714415	119306	1820	OG					
75	714386	119669	1845	OG					
76	714362	119782	1800	OG			N		
77	714366	119930	1760	OG					
78	714410	120045	1760				N		
79	714759	120908	1925	OG					
80	714892	121037	2000	PG					
81	714866	121198	2041						
82	714715	121527	2104	OG					
83	714661	121509	2106				S		
84	714619	121499	2095	OG			S		
85	714440	121458	2088	OG					
86	714274	121515	2115	OG					Shearband, normal f. to E
87	714091	121571	2153	OG					
88	713758	121767	2290						
89	713947	121851	2359	OG					
90	714023	121882	2393	OG					
91	713817	121591	2200	PG					
92	713586	121609	2150	OG					
93	713632	121386	2075	OG					
94	713600	121282	2056	PG			S		
95	713373	121012	1917						
96	713110	120847	1830						
97	712880	120279	1618	OG					
98	712378	119712	1337						
99	711982	119680	1326						
100	711432	119682	1100						
101	711283	119665	1003						
102	711288	119602	970	OG					
103	710953	119733	760	PG					
104	710835	119786	690						
105	710463	119829	675	PG					
106	710187	119968	639						
107	719431	118223	1300	OG			S		
108	719519	118246	1312						
109	719873	118518	1297	OG			S		
110	720010	118832	1284	OG					
111	720170	118977	1237	CG					
112	719979	119194	1219	OG				Yes	
113	719411	119197	1240	OG			S		
114	719271	119309	1295	OG					
115	719239	119390	1312				N		
116	718677	119502	1290						
117	718587	119574	1300				S		
118	718158	119587	1460						
119	717879	119777	1570						
120	717714	120041	1614	OG					
121	717328	120180	1765						
122	717125	120199	1840	CG					
123	716443	119953	1880	OG					
124	716038	119831	1890	OG			S		
125	716015	119744	1927	CG					
126	715947	119634	1930	OG					
127	715885	119479	2015	OG			S		
128	715746	119347	2046	OG					
129	715715	119256	1980	OG					
130	715689	119191	1934	OG			S		
131	715649	118675	1900	PG					
132	717162	120293	1857	PG					
133	717399	120358	1836	PG	9	Yes			
134	717556	120574	1845	OG					
135	717773	120643	1850			Yes	N		
137	716996	120669	2045	PG					
138	717050	120802	2014	PG					
139	716831	121292	1172	OG					
140	716945	121465	1683	PG					
141	716886	121658	1643	OG					
142	716740	121800	1620	Am		Yes			
143	716805	121841	1580	OG					
144	716748	121969	1546						
145	716897	122186	1519	OG					
146	716938	123006	1373	U					
147	716994	123201	1297	OG					
148	717030	123419	1235	OG					
149	716960	123668	1070	OG					
150	717192	123864	1007	PG					
151	717456	124335	989	PG					
152	717451	124610	913	OG					

153	719905	116237	275	PG				Yes	
154	719340	116311	417	OG					
155	719212	116319	470	OG					Shearband dextral
156	719171	116416	526	Am					
157	719065	116516	600	OG			N		
158	718951	116505	660						
159	718739	116501	746						
160	718564	116522	817	M	10a, 11				
161	718477	116542	854	Am		Yes	S		
162	718338	116510	885	CM	12				
163	718311	116628	935	OG					
164	718209	116660	998	OG					
165	718061	116758	1043	OG		Yes	S	Yes	
166	717863	116911	1103	OG				Yes	
167	717552	116893	1188	OG				Yes	
168	716757	117206	1457	OG				Yes	
169	716413	117464	1448	OG				Yes	
170	716357	117616	1446	OG			S		
171	715867	117725	1450	OG					
172	715512	117603	1445	OG					
173	715323	117671	1505	OG					
174	715204	118125	1500	OG			N		
175	715026	118625	1515	OG			SE	Yes	
176	715200	119347	1630	OG			S		
177	715149	119464	1700	OG					
178	715205	120096	1733						
179	715248	120377	1733	OG					
180	715214	120678	1990	PG					
181	715086	120922	2044	PG					
182	715070	120731	2073	CG					
183	715024	120742	2124	OG					
184	714949	120606	2144	OG					
185	714889	120479	2098	OG					
186	714812	120172	2079	OG					
187	714738	119954	2047	OG					
188	714711	119793	2038	OG					
189	714553	119188	1905	OG					
190	714211	118845	1700	OG					
191	714381	118678	1650	PG					
192	714541	118490	1604	CG					
193	714699	118378	1590	CG					
194	715788	117139	1225	OG					
195	715852	117083	1214	OG					
196	715950	117036	1160	OG					
197	715782	116843	1120	OG					
198	715782	116652	1108				S		
199	715610	116419	1090	OG					
200	716145	116378	775	OG					
201	716056	116151	713	OG					
202	716038	115968	640	OG					
203	716097	115656	565	OG				Yes	
204	716146	115358	491						
205	716244	115342	470						
206	721897	118449	250	OG			N		
207	721932	118533	360	OG			NW		
208	721874	118577	275	Am					
209	721877	118600	280	OG					
210	721812	118642	300						
211	721928	118684	320	OG					
212	722046	118690	325	OG					
213	722123	118744	325	OG			S		
214	722138	118833	340	OG			S		
215	722084	118845	380	OG			S		
216	721904	118877	440	OG					
217	721928	119018	495	OG					
218	722078	119188	520	OG			S		
219	721855	119194	578	OG			S		
220	720471	116624	258	OG					
221	720691	116743	270	OG					
222	720491	116783	335	OG			NE		
223	720273	116718	365						
224	720162	116676	365				S		
225	719996	116587	418						
226	720081	116740	625	OG					
227	720614	117095	469	OG					
228	720097	116925	510	OG					
229	722759	119545	315	OG					
230	722703	119740	400	OG			S		
231	722669	120053	418	Am					

232	722595	120375	560	OG					
233	722555	120112	475	OG					
234	722249	119918	550	OG					
235	718761	118317	1284	D					
236	718746	118264	1273	Am	13				
237	718693	117968	1209	Am					
238	718721	117853	1135	D					
239	718396	117723	1075	OG					
240	718643	117729	1045	Am			S	Yes	
241	718913	117855	1045	OG			S		
242	718961	117936	1039	OG		Yes			
243	719243	117901	1056	OG			N		
244	719585	117869	1041	OG					
245	719711	117915	1032	OG				Yes	
246	720018	118056	1021	OG		Yes	S	Yes	
248	720250	118559	1096	OG					
249	720243	118602	1106	OG					
250	720351	118728	1092	OG					
251	720480	118928	1102	OG			S		
252	720601	119009	1083	OG			S		
253	720470	118851	1064	OG					
254	720522	118844	1044	OG			NW		
255	720677	118906	1014	OG					
256	720947	119063	930	PG					
257	721121	119117	878	OG					
258	721226	119161	842	OG					
259	721356	119328	818	OG					
260	721523	119402	757	PG					
261	721515	119227	728	Am			N		
262	721426	119077	719	PG			S		
263	721426	118917	643	D					
264	721467	118848	600	PG					
265	721513	118677	510	OG			S		
266	721589	118558	408	OG					
267	721699	118570	320	OG					
268	721867	118589	309	Am					
269	711516	115126	198	OG					
270	711783	115036	196	OG					
271	711948	115013	195	OG					
272	712703	114921	220	OG					
273	713658	115067	245	PG					Vein sheared, thrust to N
274	713449	115151	325	OG					Augen, thrust to N
275	713451	115299	377	OG					
276	714024	115546	461	OG					
277	714069	115855	429	Am					
278	714164	115714	441	PG					
279	714259	115537	386	OG					
280	714380	115408	394	OG				Yes	
281	714609	115358	390	PG					
282	714831	115252	362	OG					
283	714933	115254	380	OG					
284	715152	115241	396	OG				Yes	
285	715436	115276	448	Am					
286	715694	115268	446	PG					
287	716101	115334	478	OG					
288	716558	115263	455	OG					
289	716899	115241	424	Am					
290	716892	115113	380	PG					
291	716740	115050	306	PG					
292	722219	120072	610	OG					
293	721852	120058	675	OG					
294	721480	120037	724	OG			S		
295	721384	119986	738	OG					
296	721172	119950	761	PG					
297	721331	120044	780	OG					
298	721093	120050	856	OG			S		
299	722769	119462	286	OG					
300	722853	119923	260	OG			SE		
301	722919	120345	250	OG					
302	722895	120447	250	OG					
303	722819	120612	250	Am					
304	722241	120957	260	PG					
305	722098	121130	270	MC					
306	721933	121733	260	OG					
307	721738	122244	245	OG					
308	722748	119641	320	OG		Yes		Yes	Augen, dextral
309	722607	119587	357	OG					
310	722493	119568	395	OG					
311	722429	119614	415	OG					

312	722458	119654	432	PG					
313	722312	119772	493	OG					
314	722109	119720	500	OG					
315	721835	119618	500	OG		Yes			
316	721777	119606	500	PG					
317	721696	119681	500	OG					Cataclasite, thrust to N
318	721412	119723	515	OG			N		
319	721113	119768	519	OG					
320	721146	119818	638	OG					
321	721290	119834	638	OG					
322	722465	119481	319						
323	722792	119403	310	OG					
324	722769	119304	290	OG			S		
325	721574	120408	835	OG			S		
326	721452	120496	900	OG					
327	721593	120612	805	OG					
328	721426	120778	830	OG					
329	721105	120904	920	OG					
330	720896	121048	935	PG					
331	720690	121113	980	OG					
332	720572	121080	1010	OG					
333	720440	121178	1000	PG					
334	721814	120472	740	OG			S		
335	721804	120643	700	OG					
336	721715	120743	700	Am					
337	721452	121140	660	OG		Yes			
338	709692	119899	540	OG					
339	709981	119752	505	OG		Yes	S		
340	710034	119706	540	OG		Yes	S		
341	709795	119674	501	OG					
342	709776	119232	538						
343	709710	118952	507	PG					
344	709709	118691	525	PG			S		
345	709738	118478	566						
346	709670	118259	546	OG					
347	709611	118177	526	PG					
348	709632	117917	545	PG		Yes	S		
349	709683	117815	539	OG					
350	709477	117737	495	OG					
351	709234	117468	529	PG					
352	709015	116791	489	PG					
400	716751	114953	440	OG					
401	716640	114957	445	Am		5094-5096			
402	717033	115114	545	OG	GU01		S		
403	716828	115206	585	OG					
405	721782	119136	598	OG	CA02	0001-0002	S		
406	722458	118718	240	OG	CA03				
407	722013	120304	720	OG	GO01				
408	722225	120953	260	OG	GN01				
409	722782	116149	300	OG	BE01				
410	722011	114178	265	OG	GI01				
411	722623	115199	420	OG	GI02				
412	719873	116257	280	OG	SE01				
413	714188	115107	245	OG	CU01				
414	722215	117040	225	OG	BE02				
500	721786	114234	300	PG	GI03				
501	722642	115187	420	Am	GI04		N		
502	721812	119153	580	OG	CA04		S		
503	722424	118672	260		CA05				
504	722077	120174	700	OG	GO02				
506	722231	120947	260		GN02				
507	722252	116846	260	OG	BE03				
508	723016	116910	340	OG	BE04				
509	721686	120598	780	PG	GO03				
510	722069	120193	700	PG	GO04				
511	710981	120314	993	OG					
511	720971	122690	397	OG	GN03				
512	710995	120383	1038					Yes	
514	711067	120580	1177	PG					
515	711110	120839	1310	OG					
517	711068	121035	1365	PG					
518	711077	121144	1396	PG					
519	711115	121373	1451						
520	710518	121431	1560	U	VO1,VO2				
521	711075	121989	1753	OG				Yes	
522	711231	122075	1802	OG					
523	711449	122072	1921	OG					
524	711499	122083	2045	OG					
525	711636	122280	2144	OG					

526	712011	122216	2243	OG					
527	712189	121928	2442	OG					
528	712267	121691	2320				S	Yes	
529	712358	121827	2277						
530	712590	121929	2241						
531	712737	121929	2220	PG			S	Yes	
532	712966	121743	2156	Aplite	A				
900	719894	118560	1297						
901	717675	121177	2276	PG			S		
902	717636	121259	2240	PG					
903	717655	121217	2250	PG					Shearband, thrust to S
904	717667	121180	2260	PG					
905	722328	120191	590	OG					
906	716990	120225	1868						
907	716649	120090	1930						
908	716670	119798	1770						

Table of all measurements

Nr	Typ	Info	Az	D
1	S1		156	42
1	L1		244	14
1	L2		194	46
1	L3		185	2
1	SB1	shearband, top S	155	65
2	S1		167	39
2	S2		185	49
2	S3		175	44
2	SB1	britle fault, sx	120	76
2	LB1		32	14
2	SD1		192	34
2	SD2		194	52
2	LD1		141	13
2	LD2		6	33
3	S1		175	52
3	SB1	shearband, top S	226	86
3	SB2	shearband, top S	45	76
3	SB3		228	78
4	SB1	Qtz-vein	164	56
4	SB2	top S	77	58
4	LB1		149	50
4	LB2		12	15
5	S3		215	15
5	S2		173	70
5	S1		146	60
5	S4		138	65
5	S5		158	65
5	S6		327	47
6	S1		162	57
6	S2		136	59
6	L1		233	22
6	SD1		336	25
6	SD2		170	55
6	LD1		223	2
6	LD2		202	45
7	S1		173	54
7	S2		170	52
7	S3		174	69
7	LD1		135	43
7	LD2		225	59
8	SD1		151	70
8	SD2		174	76
8	LD1		242	5
8	LD2		245	13
8	LD3		240	5
8	LD4		165	85
9	S1		339	67
9	S2		321	71
9	L1		50	34
9	L2		53	32
11	S1		175	84
11	S2		180	73
11	S3		160	80
11	SD1		180	58
11	LD1		250	1
12	S1		170	70
12	S2		186	62
12	L1	intersection	252	25
12	L2	intersection	253	34
12	L3	biotite	167	59
12	SB1	joint, chlorite	92	72
12	SD1		164	66
12	LD1		145	58
13	S1		166	65
13	SB1	shearband, top S	127	14
13	SD1		174	31
13	SD2	joint	332	27
13	LD1		96	8
14	S1		197	42
14	S2		195	36
14	S3		200	41
14	L1	biotite+qtz	265	15
14	L2	biotite+qtz	266	38
15	S1		195	84
15	L1	intersection	143	50
15	L2	biotite	96	4
15	L3	biotite	120	9
15	SD1		195	62
15	LD1		143	50
16	S1		175	34
16	S2		191	34
18	S1		182	17
18	S2		191	13
18	S3		200	36
18	L1	intersection	139	10
18	L2	intersection	120	4
19	S1		212	42
19	S2		187	7
19	S3		200	52
20	S1		211	37
20	S2		185	30
20	S3		162	52
20	SD1		266	20
20	SD2		270	18
20	SD3		236	44
20	SD3		352	64
20	SD4		337	16
20	SD5		262	6
20	LD1		260	20
20	LD1		252	31
20	LD2		258	29
20	LD3		256	26
20	LD4		242	8
20	LD5		248	3
20	LD6		245	13
21	S1		219	14
21	S2		184	38
21	S3		180	46
21	S4		178	39
21	L1	intersection	140	30
21	L2		120	10
21	L3		140	30
21	SB1	joint	70	60
21	SB2		114	9
21	SD1		255	25
21	LD1		262	15
22	S1		187	35
22	S2		161	34
22	LD1		270	5
23	S1		186	24
23	L1	intersection	118	9
24	S1		178	20
24	L1		117	6
25	S1		230	22
25	LD1		297	2
25	LD2		288	9
26	SB1		72	71
26	SB2		80	46
26	SB3		246	76
27	S1		196	28
27	SD1		208	18
27	LD1		293	9
28	S1		200	20
28	L1		120	4
29	S1		194	24
29	SB1	joint	268	89
29	LD1		274	10
30	S1		184	25
30	SD1		206	29
30	SD2		201	80
30	LD1		106	3

30	LD2		111	2
30	LD3		275	16
31	S1		173	42
31	S2		190	45
31	L1	intersection	99	27
31	L2	crenulation	108	12
31	L3	striation	270	10
31	SD1		35	77
31	LD1		108	12
32	S1		185	16
32	S2		186	49
32	S3		196	23
32	L1		128	10
32	L2		111	7
32	L3	intersection	118	6
34	S1		201	37
34	S2		200	56
34	LD1		276	18
35	S1		192	41
36	S1		198	70
37	S1		199	28
38	S1		184	47
38	SB1	shearband, top S	228	26
38	SB2	joint	86	77
38	SD1		205	26
38	LD1		260	11
38	LD2		272	26
39	S1		195	38
39	SB1	shearband, top S	224	19
40	S1		183	55
40	S2		183	30
40	L1	intersection	270	21
40	LD1		274	24
41	S1		188	51
42	S1		200	44
42	SD1		253	41
42	LD1		265	15
42	LD2		246	7
43	S1		180	55
43	S2		176	46
43	S3		142	48
43	S4		167	72
43	SB1	vertical leucosome	180	88
43	SD1		254	25
44	S1		187	80
44	LD1		170	20
44	LD2		200	35
44	LD3		260	10
45	S1		197	52
45	L1	crenulation	288	10
45	SD1		202	35
45	LD1		288	10
46	S1		187	55
46	SD1		217	31
46	LD1		240	34
46	LD2		230	30
47	S1		184	76
47	L1	biotite	87	7
48	S1		182	58
48	S2		190	72
48	SB1	top S	202	37
48	SB2	top S	197	42
48	LB1		145	13
48	LB2		140	27
49	S1		357	85
49	S2		190	60
49	S3		349	80
49	SD1		162	50
49	LD1		254	6
50	S1		183	74
50	S2		201	60
50	SD1		324	79
50	SD2		232	36
50	LD1		264	58
51	LD1		317	80
52	S1		170	60
52	SD1		142	17
52	LD1		247	8
53	S1		195	56
53	SD1		151	15
53	LD1		121	12
54	S1		164	65
54	LD1		68	7
55	S1		348	62
55	SD1		303	85
55	LD1		25	62
56	S1		344	72
57	S1		349	84
57	SD1		305	85
57	LD1		308	80
58	S1		168	80
58	S2		178	80
59	S1		180	74
60	S1		20	74
60	S2		28	82
60	S3		28	78
60	S4		24	81
60	L1		222	45
60	SB1	shearband, top N	224	66
61	S1		15	69
61	S2		22	78
61	SD1		12	80
61	LD1		121	14
62	S1		21	62
62	L1		295	10
62	LD1		295	10
65	S1		4	75
65	S2		13	64
65	L1	mineral	122	58
65	L2	intersection	96	4
65	SB1	normal fault	107	62
65	LB1		47	56
66	S1		30	54
66	SB1	normal fault	107	60
66	LB1		97	59
66	SD1		30	66
66	LD1		113	4
66	LD2		322	24
67	S1		17	78
67	S2		9	85
67	S3		15	80
67	L1	intersection	95	4
67	SB1		100	55
67	SB2		112	64
67	LB1		67	54
68	S1		190	87
69	S1		10	89
70	S1		345	58
70	S2		3	68
70	L1	intersection	250	1
71	S1		6	83
71	S2		347	89
72	S1		202	80
72	SD1		16	75
72	LD1		282	5
73	S1		185	87
73	S2		183	65
73	L1	intersection	283	11
73	L2	biotite	275	17
75	S1		144	44
75	S2		138	39
75	S3		171	45
75	L1	intersection	96	24
75	L2	biotite	128	32
75	SB1		258	36
75	S4		261	50
75	SB3		34	49
76	S1		194	44

76	S2		200	35
76	S3		182	40
76	S4		240	35
77	S1		345	70
78	S1		190	30
78	L1	biotite	102	5
78	L2		98	5
79	S1		196	15
79	S1		183	13
79	L1	biotite	305	4
79	SB1	joint	104	85
80	S1		182	13
80	S2		230	17
80	SD1		230	16
80	LD1		326	21
81	S1		188	10
82	S1		192	12
82	L1	intersection	123	5
83	S3		271	60
83	S2		235	50
83	SD1		332	70
83	LD1		308	62
83	LD2		304	74
84	S1		175	8
84	L1		115	10
84	SD1		175	8
84	LD1		115	10
84	LD2		117	11
85	S1		176	4
85	LD1		284	2
86	S1		173	11
86	L1	intersection	120	9
86	SB1	dn	97	66
86	SB2	joint	282	86
87	S1		117	2
87	L1	intersection	117	2
88	S1		100	10
88	S2		120	10
88	L1	mineral	113	10
89	S1		120	9
89	L1		109	9
90	S1		144	4
91	S1		270	10
92	S1		137	14
92	SB1	joint	88	78
93	S1		153	27
93	L1	intersection	114	20
94	S1		145	12
94	L1		116	11
94	SD1		146	14
94	LD1		99	20
95	S1		145	11
96	S1		113	11
97	S1		122	14
98	S1		181	36
98	L1	intersection	100	4
99	S1		173	26
100	S1		192	55
101	S1		193	56
101	L1		113	2
102	LD1		100	14
103	S1		203	56
103	L1		116	9
104	S1		205	65
105	S1		192	70
105	L1	intersection	103	1
105	L2	mineral+intersection	48	17
107	S1		348	33
107	S2		335	45
107	SD1		336	60
107	LD1		58	16
108	S1		344	32
108	L1	intersection	48	26
108	SD1		344	32
108	LD1		37	20
109	S1		338	61
109	S2		339	80
109	S3		350	65
109	S4		8	73
109	SD1		338	61
109	LD1		55	20
110	S1		340	85
110	S2		354	74
110	L1		76	9
110	LD1		76	9
111	S1		179	83
112	S3		176	41
112	S1		168	65
112	LD1		96	29
113	S1		354	84
113	LD1		83	19
114	S1		140	89
115	S1		140	89
115	SD1		160	89
115	LD1		268	46
115	LD2		260	58
116	S1		193	80
117	S1		143	78
117	L1	intersection	232	11
117	L2	intersection	42	2
117	LD1		41	3
118	S1		188	65
118	SB1	joint	85	75
118	SB2	joint	80	76
119	S1		182	63
119	S2		195	58
120	S1		334	87
120	S2		68	28
121	S1		198	68
121	S2		186	40
121	L1		113	6
121	LD1		260	8
122	S1		201	79
122	L1	biotite	124	20
123	S1		194	31
123	L1	intersection	140	11
124	S1		195	32
124	L1	biotite	125	14
124	LD1		93	9
124	LD2		90	11
125	S1		205	36
125	S2		173	20
126	S1		176	27
126	S2		190	33
126	LD1		72	82
127	S1		190	45
127	SD1		238	20
127	LD1		280	21
127	LD2		292	19
128	S1		227	55
128	S2		236	52
128	LD1		309	18
128	LD2		309	12
129	S1		196	52
130	S1		200	59
130	SD2		205	75
130	LD1		280	6
131	S1		6	84
132	S1		198	35
132	S2		174	56
132	L1	intersection	112	1
132	L2		115	15
133	S1		202	68
133	S2		223	70
133	S3		206	75
133	L2		120	20
133	L3		113	20
133	L1		290	3

133	LD1		292	8
133	LD2		114	11
134	S1		41	84
135	S1		40	62
135	SB1		152	23
135	SB2	joint	300	85
135	SB3	joint	106	82
135	LB1		84	6
135	LD1		126	19
137	S1		204	46
137	S2		165	24
137	L1	mineral	108	15
138	S1		220	19
138	L1		303	12
138	LD1		127	10
139	S2		40	65
139	L2	intersection	128	6
140	S1		214	20
141	S1		230	38
141	S2		216	25
141	S3		204	12
141	L1		149	10
142	S1		205	21
142	L1	biotite	137	8
142	SB1	joint	285	87
142	SB2		112	71
142	SB3		121	68
143	S1		200	20
143	S2		217	27
143	L1	mineral	285	10
143	L2	intersection	142	14
144	S1		182	26
144	L1		143	25
144	SD1		226	50
144	LD1		127	1
144	LD2		137	13
145	S1		213	27
145	L1	mineral	151	8
146	S1		170	20
146	S2		178	54
147	S1		188	26
147	L1		200	8
148	S1		185	25
149	S2		198	50
150	S1		206	15
150	L1	biotite	125	2
151	S1		202	31
151	L1		147	18
151	L2	vertical striation	190	64
152	S1		217	22
153	S1		339	82
153	S2		313	76
154	S1		329	84
154	S2		160	88
154	L1	biotite	70	36
154	SB1	cracks (cm) in qtz	210	89
154	SD1		322	81
154	LD1		282	60
155	S1		339	80
155	S2		337	78
155	SB1	joint	106	60
155	SB2	joint	258	80
155	SB3	shearband	174	75
156	S1		315	63
156	L1	biotite	66	20
157	S1		319	86
157	L1	intersection+mineral	58	12
157	LD1		44	45
158	S1		330	72
158	S2		320	80
158	SD1		148	72
158	LD1		247	35
159	S1		303	57
160	S2		321	25
160	S2		304	56
160	S3		307	56
161	SD1		329	63
161	LD1		49	18
162	S1		340	67
163	S1		337	74
163	L1	intersection	44	52
164	S1		347	60
164	L1		43	41
165	S1		351	61
165	LD1		85	4
165	LD2		45	5
165	LD3		347	83
166	S1		337	89
166	S2		350	78
166	L1	biotite	70	3
167	S1		345	70
167	L1	mineral	63	22
168	S1		168	80
168	L1	biotite	82	1
169	S1		167	75
169	L1	intersection	200	2
170	S1		356	78
170	L1		100	11
170	LD1		80	40
171	S1		191	79
172	S1		189	80
173	S1		187	85
174	S1		175	80
174	S2		184	78
174	L1	intersection	90	18
174	L2	intersection	275	8
174	LD1		257	52
175	S1		193	80
175	L1		101	21
175	SB1	joint	85	89
176	S1		185	42
176	SB1	joint	75	87
176	LD1		269	8
177	S1		186	35
177	SB1	joint	244	87
178	S1		197	40
178	SB1	joint	293	70
179	S1		197	38
179	L1		106	13
180	S1		176	16
180	L1	mineral	118	9
181	S1		212	18
181	L1		292	1
182	S1		212	24
183	S1		0	30
183	SB1	joint	286	89
184	S1		211	26
184	L1	mineral	101	14
185	S1		201	27
185	S2		203	62
186	S1		218	30
187	S1		172	41
187	L1		135	20
188	S1		195	45
188	L1	biotite	121	8
188	LD1		281	15
189	S1		197	60
190	S1		3	73
190	S2		5	51
191	S1		0	27
192	S1		224	30
193	S1		194	30
193	L1		100	4
193	SB1	qtz vein	108	25
193	SB2	joint	10	75
193	SB3	joint, chlorite	89	78
193	SD1		173	72
193	LD1		80	52

194	S1		174	70
194	L1	mineral	86	11
195	S1		10	73
196	S1		11	86
196	S2		350	80
197	S1		349	65
197	S2		5	78
198	S1		184	88
199	S1		348	84
200	S1		357	76
200	L1	intersection	80	23
200	L2	biotite	81	6
201	S1		7	78
201	S2		350	50
201	L1	intersection	96	23
202	S1		177	88
202	SB1	joint	200	18
203	S1		340	70
203	L1		60	24
203	SD1		348	68
203	LD1		78	2
204	S1		350	66
204	LD1		349	73
204	LD2		263	35
205	S1		348	78
206	S1		215	87
206	SD1		27	80
206	LD1		188	64
207	S1		156	85
207	L1	intersection	67	45
207	L1	mineral	132	80
207	SD1		169	76
207	LD1		71	79
208	S1		173	89
208	L1	intersection	82	63
209	S1		5	88
209	S2		26	89
209	L1	biotite	290	62
210	S1		38	52
211	S1		194	89
211	S2		188	40
211	L1	biotite	105	9
211	SD1		134	58
211	LD1		237	28
212	S1		166	81
212	L1	intersection	131	78
212	LD1		130	75
213	S1		335	85
213	LD1		74	26
214	S1		170	83
214	LD1		71	26
215	S1		155	87
215	SD1		157	78
215	LD1		78	27
216	S1		156	87
216	L1	intersection	80	11
216	SD1		349	85
216	LD1		91	11
217	S1		161	86
217	L1	intersection	69	47
217	SB1	shearband, top S	175	40
217	SD1		98	28
218	S1		192	71
219	S1		13	79
219	S2		164	85
219	SD1		199	88
219	LD1		90	12
219	LD2		219	87
220	S1		327	71
220	L1	intersection	55	27
221	S1		321	79
221	LD1		55	30
222	S1		328	76
222	L1		55	25
222	SB1	joint, N up	58	88
222	SD1		337	78
222	LD1		55	66
223	S1		339	76
223	LD1		56	49
224	S2		350	57
224	LD2		98	26
225	S1		351	66
225	LD1		87	14
226	S1		339	72
226	LD1		35	85
227	S1		352	79
228	S1		350	82
229	S1		178	73
229	S2		165	88
229	L1	biotite	82	78
229	L2	intersection	79	40
229	SB1	shearband	30	85
230	S1		180	81
230	SB1	shearband	213	79
230	SB2	shearband	214	50
231	S1		190	81
232	S1		194	85
232	S2		205	89
233	S1		167	78
233	S2		208	88
234	S1		178	79
234	L1	mineral	195	64
235	S1		337	70
235	S1		132	76
236	S1		332	42
236	S2		343	52
237	S1		330	45
238	S1		0	30
239	S1		343	38
240	S1		25	22
240	L1		103	3
241	S1		346	65
241	LD1		265	5
242	S2		177	80
242	L2	biotite	260	43
242	L2		260	1
243	S1		0	48
243	SB1		108	70
243	SB2		222	38
243	LD1		260	5
244	S1		355	42
245	S1		342	35
245	S1		25	4
246	S2		176	8
246	L2		88	20
247	S1		337	60
247	L1		220	13
248	S1		348	68
249	S1		147	87
250	S1		353	78
251	S1		353	68
251	LD1		88	1
252	S1		337	85
253	S1		160	78
254	S1		350	74
254	L1		77	34
254	LD1		90	0
255	S1		350	86
255	SB1		86	64
255	SB2	vein	280	76
256	S1		167	90
256	L1		75	50
257	S1		160	84
258	S1		162	78
259	S1		161	74
260	S1		161	86
261	S1		329	77
261	LD1		254	30

262	S1		162	85
263	S1		342	90
264	S1		350	89
265	S1		13	82
266	S1		167	65
267	S1		136	88
268	S1		166	84
268	L1		166	84
269	S1		11	68
270	S1		13	82
270	LD1		108	8
270	L1	glacier	264	20
271	S1		333	68
272	S1		324	50
272	L1		261	24
273	S1		12	61
273	L1	feldspar	305	27
273	SB1	quartz	90	84
274	S1		349	59
274	L1		276	20
275	S1		348	52
275	L1	mica	243	28
276	S1		351	50
276	SB1		188	86
277	S1		6	82
278	S1		1	85
278	S1		188	60
279	S1		336	58
280	S1		8	76
280	LD1		91	38
280	LD2		90	4
281	S1		352	88
282	S1		347	69
282	L1		255	9
283	S1		350	50
283	LD1		12	40
284	S1		342	58
285	S1		354	85
286	S1		348	66
287	S1		325	85
288	S1		319	85
289	S1		333	75
290	S1		180	55
291	S1		335	57
292	S1		197	74
293	S1		167	68
293	L1	intersection	248	35
294	S1		175	84
294	S2		123	54
294	L1	biotite	124	82
294	SB1	shearband, top NE	25	66
295	S1		182	80
295	SD1		337	81
295	LD1		193	86
296	S1		171	83
296	S2		168	79
296	L1	mineral	88	45
297	SD1		34	35
297	LD1		339	19
298	S1		340	70
298	SB1	joint	94	65
300	S1		357	88
301	S1		190	69
301	L1	biotite	135	56
302	S1		180	70
302	L1	biotite	267	3
302	L2	intersection	90	59
302	SB1	major fault	175	85
303	S1		193	76
303	S2		184	78
303	L1		117	42
304	S1		160	55
304	SB1	shearband, top N	161	40
305	S1		168	89
305	S2		185	69
305	S3		168	83
305	L1	striation	75	3
305	SD1		201	80
306	S1		180	71
306	S2		168	68
307	S1		166	71
308	S1		18	83
308	S2		339	74
308	L1	mineral	102	7
308	L2	stretching	280	69
309	S1		352	73
309	L1	intersection	78	20
310	S1		17	79
310	L1	strong lineament	309	68
311	S1		166	87
313	S1		155	72
313	L1	intersection	113	68
313	SB1		68	35
314	S1		194	82
314	LD1		128	71
315	S1		168	70
316	S1		190	85
317	S1		192	78
317	SB1	cataclasite	55	60
318	S1		170	79
319	S1		170	83
320	S1		346	88
321	S1		184	82
322	S1		186	76
323	S1		172	81
324	S1		160	90
325	S1		168	79
325	S2		172	81
325	L2	intersection	96	60
326	S1		169	80
326	L1	biotite	111	39
326	L2	biotite	124	58
327	S1		195	73
328	S1		205	65
329	S1		45	83
329	LD1		126	28
330	S1		197	85
330	S2		210	84
331	S1		162	55
332	S1		190	70
333	S1		174	62
334	S1		176	65
334	L1	intersection	108	72
335	S1		190	65
335	L1	intersection	133	55
336	S1		188	79
337	S1		205	85
338	S1		192	79
338	L1	crenulation	100	9
338	L2	biotite	120	34
338	SB1		283	75
338	LB1		261	74
339	S1		190	70
339	L1	also fold axis	112	12
340	S1		198	76
340	LD1		106	10
340	SD1		198	40
341	S1		195	78
341	L1		113	9
342	S1		194	88
343	S1		201	73
343	S2		190	90
343	L1	open crenulation	101	11
344	S1		185	74
344	L1	biotite	99	8
345	S1		191	90
346	S1		17	80
347	S1		193	85

347	LD1	crenulation	105	3
348	S1		14	82
348	LD1		101	10
349	S1		0	80
349	L1		95	6
350	S1		19	78
351	S1		16	85
352	S1		0	70
400	S1		354	6
400	L1	mineral	81	85
400	S2		354	65
400	L1	mineral	81	14
401	S1		348	68
401	L1		251	9
402	S1	N side up	326	41
402	S2		330	40
403	S1		350	53
404	S1		357	81
404	L1	biotite	328	73
405	S1		185	86
405	SD1		169	82
405	LD1		275	35
405	S2		354	80
405	L1	biotite	69	65
406	SD1		348	71
406	LD1		247	25
406	S1		345	87
406	L1		67	46
407	S1		186	78
407	L1		98	35
408	S1	no lineation	164	60
409	S1		316	83
409	L1	biotite	38	12
409	L2	biotite	12	68
410	S1		333	47
410	L1	biotite	298	44
411	S1		153	85
411	L1	plag	235	26
411	SD1		158	56
411	LD1		222	38
412	S1		328	78
412	L1		63	5
413	S1		348	63
413	L1	biotite	14	55
414	S1		337	78
414	L1	mineral	45	38
500	S1		178	80
500	S2		358	85
500	L1		80	27
501	S1		160	55
501	L1		248	15
501	SD1		152	51
501	LD1		222	35
502	S1		174	79
502	L1		90	7
503	S1		354	85
511	S1		190	48
511	L1	intersection	110	26
512	S1		180	40
512	L1	intersection	121	19
514	S1		180	32
514	L1	intersection	121	19
515	S1		186	30
515	S2		145	20
515	L1		125	17
515	SB1		290	73
517	S1		130	21
518	S1		130	18
519	S1		93	16
519	L1	intersection	140	9
521	S1		115	14
521	L1	mineral	142	12
522	SB1	Joint with pegmatite	284	35
522	S1		112	23
522	SB2	slickenside	282	33
522	LB2	normal fault	270	33
522	SB3	joint	242	76
523	S1		104	22
524	S1		63	14
524	L1		105	11
525	S1		109	12
525	L1		125	9
526	S1		109	8
527	S1		115	8
527	L1		112	6
528	S1		160	7
529	LD1		112	8
530	S1		182	37
530	LD1		101	6
531	S1		114	22
901	S1		157	19
901	L1	biotite	85	5
901	L1	intersection	105	10
901	SD3		213	60
902	S1		200	20
902	L1	intersection	107	2
902	SB1	joint	321	78
902	LD1		125	20
903	S1		208	15
903	S4		200	15
903	S2		230	44
903	S6		221	31
903	SB2	shearband	224	2
903	SD2		207	15
903	LD2		113	12
904	S1		220	66
904	S8		221	76
904	LD3		130	17
905	S1		185	76
905	L1	intersection	115	65
906	S2		175	46
906	S1		179	20
906	L4		90	4
907	S2		200	33
907	LD1		261	24
908	S2		200	21

Eidgenössische Technische Hochschule Zürich
Swiss Federal Institute of Technology Zurich

Declaration of originality

The signed declaration of originality is a component of every semester paper, Bachelor's thesis, Master's thesis and any other degree paper undertaken during the course of studies, including the respective electronic versions.

Lecturers may also require a declaration of originality for other written papers compiled for their courses.

I hereby confirm that I am the sole author of the written work here enclosed and that I have compiled it in my own words. Parts excepted are corrections of form and content by the supervisor.

Title of work (in block letters):

3D geometry and deformation of the Maggia Nappe and the transition to the Southern Steep Belt

Authored by (in block letters):

For papers written by groups the names of all authors are required.

Name(s):	**First name(s):**
Winterberg	Sascha

With my signature I confirm that

- I have committed none of the forms of plagiarism described in the 'Citation etiquette' information sheet.
- I have documented all methods, data and processes truthfully.
- I have not manipulated any data.
- I have mentioned all persons who were significant facilitators of the work.

I am aware that the work may be screened electronically for plagiarism.

Place, date	**Signature(s)**

For papers written by groups the names of all authors are required. Their signatures collectively guarantee the entire content of the written paper.